Title: Epithelial endoplasmic reticulum stress orchestrates a protective IgA response

Joep Grootjans[1,2†], Niklas Krupka[1,3†], Shuhei Hosomi[1,4†], Juan D. Matute[1,5], Thomas Hanley[1], Svetlana Saveljeva[6], Thomas Gensollen[1], Jarom Heijmans[2], Hai Li[3], Julien P. Limenitakis[3], Stephanie C. Ganal-Vonarburg[3], Shengbao Suo[7], Adrienne M. Luoma[8], Yosuke Shimodaira[9], Jinzhi Duan[1], David Q. Shih[9], Margaret E. Conner[10], Jonathan N. Glickman[11], Gwenny M. Fuhler[12], Noah W. Palm[13], Marcel R. de Zoete[14], C. Janneke van der Woude[12], Guo-Cheng Yuan[7], Kai W. Wucherpfennig[8], Stephan R. Targan[9], Philip Rosenstiel[15], Richard A. Flavell[13], Kathy D. McCoy[16], Andrew J. Macpherson[3], Arthur Kaser[5], Richard S. Blumberg[1*]

Affiliations:

[1] Division of Gastroenterology, Department of Medicine, Brigham and Women's Hospital, Harvard Medical School, 75 Francis Street, Boston, MA 02115, USA

[2] Amsterdam University Medical Center, University of Amsterdam, Department of Gastroenterology and Hepatology & Tygat Institute for Liver and Intestinal Research, Meibergdreef 9, Amsterdam, Netherlands

[3] Maurice Müller Laboratories (DBMR), Universitätsklinik für Viszerale Chirurgie und Medizin Inselspital, Murtenstrasse 35, University of Bern, 3010 Bern, Switzerland

[4] Department of Gastroenterology, Osaka City University Graduate School of Medicine, 1-4-3, Asahi-machi, Abeno-ku, Osaka 545-8585, Japan

[5] Division of Neonatology, Department of Pediatrics, Massachusetts General Hospital, Harvard Medical School, Boston, MA 02114, USA

[6] Division of Gastroenterology and Hepatology, Department of Medicine, University of Cambridge, Cambridge CB2 0QQ, United Kingdom[s7] Department of Biostatistics and

Computational Biology, Dana-Farber Cancer Institute and Harvard T. H. Chan School of Public Health, Boston, MA 02215, USA

[8] Department of Cancer Immunology and Virology, Dana-Farber Cancer Institute, 450 Brookline Avenue, Boston, MA 02215, USA.

[9] F. Widjaja Foundation, Inflammatory Bowel and Immunobiology Research Institute, Cedars-Sinai Medical Center, Los Angeles, CA 90048, USA

[10] Department of Molecular Virology and Microbiology, Baylor College of Medicine, Houston, Texas, USA

[11] Department of Pathology, Beth Israel Deaconess Medical Center, Boston, MA 02215, USA

[12] Department of Gastroenterology and Hepatology, Erasmus MC-University Medical Centre Rotterdam, Netherlands

[13] Department of Immunobiology, Yale University School of Medicine, New Haven, CT 06519, USA

[14] Department of Infectious diseases and Immunology, Faculty of Veterinary Medicine, Utrecht University, Netherlands

[15] Institute of Clinical Molecular Biology, Christian-Albrechts-University Kiel, Rosalind-Franklin-Str. 12, 24105 Kiel, Germany

[16] Department of Physiology and Pharmacology, University of Calgary, Calgary, Canada

† These authors contributed equally to this work.

* Correspondence to: rblumberg@bwh.harvard.edu

One sentence summary: ER stress-induced IgA protects from enteritis

Abstract

Immunoglobulin A (IgA) is the major secretory immunoglobulin isotype at mucosal surfaces, where it regulates microbial commensalism and excludes luminal factors from contacting intestinal epithelial cells (IECs). IgA is induced by T cell-dependent and -independent (TI) pathways. However, little is known about TI regulation. We report that IEC endoplasmic reticulum (ER) stress induces a polyreactive IgA response, which is protective against enteric inflammation. IEC ER stress causes TI and microbiota-independent expansion and activation of peritoneal B1b cells, which culminates in increased LP and luminal IgA. Increased numbers of IgA-producing plasma cells are observed in healthy humans with defective autophagy, who are known to exhibit IEC ER stress. Upon ER stress, IECs communicate signals to the peritoneum that produce a barrier-protective TI IgA response.

Main text

The intestinal epithelium is continuously confronted with potentially deleterious environmental stimuli (*1*). These exposures and the underlying secretory burden of intestinal epithelial cells (IECs) are challenging for this cell type. Thus endoplasmic reticulum (ER) stress and the accompanying unfolded protein response (UPR) are commonly observed in IECs under homeostasis (*2*) and increased in inflammatory bowel disease (IBD) (*3, 4*). In IBD, ER stress in the IEC can serve as a nidus for spontaneous microbiota-dependent ileitis. This can be seen in mice with an IEC-restricted deletion of the important UPR effector molecule X box binding protein-1 ($Xbp1^{\Delta IEC}$) (*3, 5*). It is unknown however whether IEC-associated ER stress can also elicit barrier-protective immune responses.

We observed elevated numbers of IgA^+ plasma cells ($CD45^+CD3^-IgA^+B220^-$) in small-intestinal lamina propria (SI LP) and increased concentrations of ileal tissue IgA in $Xbp1^{\Delta IEC}$ mice compared to littermate $Xbp1^{fl/fl}$ controls (Fig. 1A and B, Fig. S1). Secretory (s)IgA, which functions to protect the mucosa by coating and entrapping commensal and colitogenic bacteria (*6*) and excluding intraluminal factors from IEC contact (*7, 8*), was also increased in the lumen (Fig. 1C). This was associated with increased circulating IgA levels as early as 6 weeks of age (Fig. 1D), prior to the emergence of spontaneous inflammation in $Xbp1^{\Delta IEC}$ mice. No other Ig isotypes were increased in the SI (Fig. S2A) or sera (Fig. S2B) of $Xbp1^{\Delta IEC}$ mice. The increased number of IgA^+ cells in $Xbp1^{\Delta IEC}$ mice accumulated around SI crypts (Fig. 1E and F), where ER stress (*5, 9*) and basal plasmacytosis, a feature of IBD (*10*), frequently occurs.

Xbp1 deletion in IECs results in UPR activation including the ER-stress sensor inositol-requiring enzyme 1 α (IRE1α) (*11*). Double conditional knockout mice lacking both IRE1α and XBP1 in IECs ($Ern1/Xbp1^{\Delta IEC}$) showed no increase in SI IgA^+ cell numbers compared to $Ern1/Xbp1^{fl/fl}$

controls (Fig. S3), indicating that IRE1α is an important mediator of the IgA response. We extended these observations to an inducible IEC-specific knockout of the ER-stress sensor glucose related protein 78 (GRP78) (*12*). *Grp78*$^{T\text{-}\Delta IEC}$ mice exhibited a rapid increase in SI IgA^{+} plasma cells by 3 days after *Grp78* deletion (Fig. 1G). Conversely, treatment of *Xbp1*$^{\Delta IEC}$ mice with the chemical chaperone tauroursodeoxycholic acid (TUDCA) (*13*) reduced IEC ER stress (Fig. S4) and prevented the IgA response in the SI LP (Fig. 1H) and plasma (Fig. 1I).

We next generated *Igha*$^{-/-}$*Xbp1*$^{\Delta IEC}$ mice and *Igha*$^{-/-}$*Xbp1*$^{fl/fl}$ controls. Consistent with previous studies (*3*), *Xbp1*$^{\Delta IEC}$ mice developed spontaneous ileitis, which was unchanged under conditions of IgA deficiency (Fig. 1J). However, inflammation in *Igha*$^{-/-}$*Xbp1*$^{\Delta IEC}$ mice significantly extended proximally into the jejunum (Fig. 1K and Fig. S5, histology score and H&E, respectively), suggesting that IEC ER stress–induced IgA^{+} plasma cells protect from inflammation. Like humans with selective IgA deficiency (*14*), *Igha*$^{-/-}$ mice exhibited a compensatory increase of LP IgM^{+} plasma cell numbers that was further elevated with IEC ER stress (*Igha*$^{-/-}$*Xbp1*$^{\Delta IEC}$, Fig. 1L). We thus generated B cell–deficient *Xbp1*$^{\Delta IEC}$ mice (*μMT Xbp1*$^{\Delta IEC}$), lacking intestinal LP plasma cells (IgA IHC shown in Fig. S6). These animals showed no significant worsening of inflammation in either the jejunum or ileum compared to *Igha*$^{-/-}$*Xbp1*$^{\Delta IEC}$ controls (Fig. 1K and S5, histology scores and H&E, respectively), indicating that in mice, compensatory IgM did not contribute to protection. This was likely due to its relatively low levels compared to IgA (Fig. S7), a reduced ability of IgM to bind several typical IgA targets (*15*), and/or differences in sIgM function in mice compared to humans (*16*). Further, the elevated numbers of IgA^{+} plasma cells in *Xbp1*$^{\Delta IEC}$ mice were not due to increased levels of interleukin (IL)-10, which can be produced by B cells (*17*)—SI tissue from *μMT Xbp1*$^{\Delta IEC}$ and *Xbp1*$^{\Delta IEC}$ mice or *Xbp1*$^{\Delta IEC}$ mice crossed with an IL-10-GFP reporter line (Vert-X) exhibited

similar levels of IL-10 (Fig. S8A) and/or frequencies of reporter^{+} LP B cells (Fig. S8B) compared to their respective littermate controls.

We examined if luminal IgA secretion was required for the protective role observed by generating a polymeric immunoglobulin receptor/*Xbp1* double-deficient mice (*Pigr*$^{-/-}$*Xbp1*$^{\Delta IEC}$), which are unable to transport IgA and IgM across the IEC (*18*). *Pigr*$^{-/-}$ *Xbp1*$^{\Delta IEC}$ mice showed an increase of LP IgA^{+} plasma cells similar to *Xbp1*$^{\Delta IEC}$ animals (Fig. 1M and N), but still developed severe inflammation of the proximal SI (Fig. 1O and Fig. S5, histology scores and H&E, respectively). This phenocopied *Igha*$^{-/-}$*Xbp1*$^{\Delta IEC}$ and *μMT Xbp1*$^{\Delta IEC}$ animals and indicated a protective role for sIgA in this model. Although *Xbp1*$^{\Delta IEC}$ animals exhibited increased IgA coating of fecal bacteria compared to *Xbp1*$^{fl/fl}$ controls (Fig. 1P), IgA-SEQ (*6*) revealed no major differences between *Xbp1*$^{\Delta IEC}$ and *Xbp1*$^{fl/fl}$ mice in the taxa-specific coating of commensal bacteria with IgA, suggesting a specific IgA-targeted microbe was not responsible (Fig. S9).

Intestinal IgA^{+} plasma cells can differentiate via T cell-dependent (TD) and T cell-independent (TI) pathways (*19, 20*). Although we observed a small increase in germinal center B cells (B220^{+}CD19^{+}CD95^{+}GL7^{+}) in Peyer's patches (PP) of *Xbp1*$^{\Delta IEC}$ mice compared to *Xbp1*$^{fl/fl}$ controls (Fig. 2A), TD pathways were not involved in the IgA induction. First, T follicular helper cell percentages (Tfh, CD3^{+}CD4^{+}ICOS^{+}PD-1^{hi}CXCL5^{hi}) (*7*) were similar in the PP and mesenteric lymph nodes (MLN) of *Xbp1*$^{\Delta IEC}$ mice compared to *Xbp1*$^{fl/fl}$ controls (Fig. 2B). Second, T cell receptor β-deficient *TCRβ*$^{-/-}$*Xbp1*$^{\Delta IEC}$ mice exhibited increased SI LP IgA^{+} plasma cell numbers (Fig. 2C) without changes in LP γδ T cells (Fig. S10) compared to *TCRβ*$^{-/-}$*Xbp1*$^{fl/fl}$ controls. Finally, PP-deficient (PP^{def}) *Xbp1*$^{\Delta IEC}$ (*21*) continued to exhibit increased SI LP IgA^{+} plasma cells (Fig. 2D) without proximal extension of SI inflammation (Fig. S11), compared with PP^{def}*Xbp1*$^{fl/fl}$ littermate controls.

In contrast, we observed increased percentages and numbers of B1b ($CD5^{-}CD19^{+}CD23^{-}CD43^{+}$), but not B1a ($CD5^{+}CD19^{+}CD23^{-}CD43^{+}$), cells in the peritoneal cavities of *Xbp1*$^{\Delta IEC}$ mice compared to *Xbp1*$^{fl/fl}$ littermate controls (Fig. 2E and 2F). B1 cells associated with TI pathways emerge and migrate from there to the intestine giving rise to polyreactive IgA-producing plasma cells in the SI (*19, 22, 23*). As this suggested a transmissible factor, we conducted parabiosis experiments in which $CD45.1^{+}$ wild-type (wt) mice were joined to $CD45.2^{+}$ *Xbp1*$^{\Delta IEC}$ mice or *Xbp1*$^{fl/fl}$ controls (Fig. 2G). Three weeks after parabiosis, we observed T and B cell chimerism in blood of ~50% (Fig. 2H). Consistent with their tissue-resident phenotype, peritoneal B1 cells exhibited ~20% chimerism (Fig. 2H). The peritoneal B1 cell compartments of wt CD45.1 mice showed increased numbers of $CD45.1^{+}$ B1b cells in animals joined to $CD45.2^{+}$ *Xbp1*$^{\Delta IEC}$ mice compared to those joined to $CD45.2^{+}$ *Xbp1*$^{fl/fl}$ controls (Fig. 2I, gating strategy in Fig. S12). There were also more $CD45.1^{+}$ IgA^{+} plasma cells in the SI LP of $CD45.2^{+}$ *Xbp1*$^{\Delta IEC}$ mice compared to $CD45.2^{+}$ *Xbp1*$^{fl/fl}$ controls, which lacked ER stress in their intestinal epithelium (Fig. 2J). In contrast, $CD45.1^{+}IgA^{+}$ plasma cells in the LP of $CD45.1^{+}$ animals were not increased (Fig. 2K). Notably, there were no significant changes in SI *Tnfsf13* (*April*), *Tnfsf13b* (*Baff*), *Ccl25*, *Ccl28* and *Cxcl13* (Fig. S13A) expression or TSLP protein levels. (Fig. S13B), which have been implicated in TI IgA class switching and/or plasma-cell recruitment (*24*).

Germ-free (GF) *Xbp1*$^{\Delta IEC}$ mice, compared to GF *Xbp1*$^{fl/fl}$ controls, also exhibited increased numbers of SI IgA^{+} plasma cells (Fig. 3A and B), basal plasmacytosis (Fig. 3B), higher frequencies and numbers of peritoneal B1b cells (Fig. 3C and D), and an elevated proportion of IgA^{+} cells among the SI LP B1b-like cell compartment ($CD5^{-}CD19^{+}CD43^{+}$) (Fig. 3F). They also showed heightened IEC ER stress (Fig. S14A–C) without spontaneous enteritis (*5*) and few SI epithelial apoptotic events compared to SPF *Xbp1*$^{\Delta IEC}$ mice (Fig. S14D). GF *Xbp1*$^{\Delta IEC}$ mouse

149 colons also showed increased numbers of IgA^+ plasma cells (Fig. S15A) and higher levels of
150 tissue IgA (Fig. S15B) compared to littermate controls. However, colonic IgA^+ plasma cell
151 numbers and IgA tissue levels in SPF *Xbp1*$^{\Delta IEC}$ and *Xbp1*$^{fl/fl}$ mice were similar (Fig. S15A and
152 B), suggesting that high levels of TD IgA production in the colon mask the TI ER stress-induced
153 IgA response under SPF conditions (*25*).

154 Thus, the increase in IgA^+ plasma cells was not restricted to the SI nor dependent on apoptosis,
155 microbiota, or a pro-inflammatory milieu but, rather, was due to IEC ER stress-driven
156 recruitment of TI peritoneal B1b cells. Indeed, although single-cell RNA sequencing (RNA-seq)
157 of the peritoneal lavage of GF *Xbp1*$^{\Delta IEC}$ mice and *Xbp1*$^{fl/fl}$ controls identified heterogenous
158 populations of peritoneal myeloid and T cell subsets (Fig. 3F–H and Fig. S16A–B), the only
159 peritoneal cell type demonstrating a major expansion in the context of IEC ER stress was a
160 cluster containing a B1b-like transcriptional signature (cluster 2, Fig. 3F–H and Fig. S16A–B).
161 Flow cytometry confirmed absence of peritoneal myeloid or T cell alterations (Fig. S17) or
162 changes in SI LP myeloid cell populations (Fig. S18). Peritoneal B1b cells from GF *Xbp1*$^{\Delta IEC}$
163 mice were also transcriptionally distinct. Differential expression (Fig. 3I) and gene set
164 enrichment analysis (GSEA, Fig. 3J) of purified B1b cells from GF *Xbp1*$^{\Delta IEC}$ mice showed the
165 upregulation of genes involved in protein biosynthesis, oxidative phosphorylation, and Myc
166 signaling—which is critical for B cell activation (*26*)—compared to GF littermate controls. In
167 contrast, cell adhesion gene sets were downregulated in line with the increased ability of these
168 B1b cells to egress from the peritoneal cavity and home to ER-stressed SI epithelium (Fig 3J).
169 Taking advantage of the increased circulating IgA levels present in GF *Xbp1*$^{\Delta IEC}$ mice compared
170 to GF *Xbp1*$^{fl/fl}$ mice (Fig. 3K), we functionally confirmed the B1 origin of the IgA response by
171 showing the IgA derived from these animals efficiently coated fecal microbiota obtained from

172 *μMT* mice lacking immunoglobulins (Fig. 3L) and exhibited broad reactivity to endogenous and
173 exogenous antigens (Fig. 3M) as expected (*23, 25*). Furthermore, analysis of variable-region
174 usage and CDR3 clonotype sequences from the proximal and distal intestinal segments of GF
175 animals demonstrated the existence of a similar IgA^+ cell polyclonal repertoire (Fig. S19A–C)
176 containing a limited CDR3 region mutational load (Fig. S19D) regardless of genotype.
177 Lastly, mice with a conditional deletion of *Atg16l1* in IECs ($Atg16l1^{\Delta IEC}$) exhibit SI IEC ER
178 stress without histopathologic signs of inflammation (*5, 11*). These animals exhibited increased
179 numbers of SI LP IgA^+ cells (Fig. 4A) and a specific increase in peritoneal B1b cells (Fig. 4B).
180 Similarly, SI biopsies of healthy human subjects homozygous for the hypomorphic
181 $ATG16L1^{T300A}$ variant, who are known to exhibit increased ER stress (*27*), exhibited increased
182 numbers of LP IgA^+ cells compared to both non-carriers and heterozygous subjects (Fig. 4C).

183 Thus, the secretion of IgA into the lumen and resultant innate-like polyreactive responses protect
184 ER-stressed mucosa in a pathway under the control of IEC ER stress. This occurs independently
185 of either microbes or inflammation, making it a self-contained, host-derived response. This
186 response is TI, peritoneal B1b cell-derived, and under the control of an unknown transmissible
187 factor that emerges from ER stress in the IEC and is communicated to the peritoneal cavity,
188 revealing a tight link between these two anatomic sites. In the absence of IgA or its secretion,
189 spontaneous enteritis emerges. We propose that this homeostatic function of epithelial ER stress
190 is a beneficial "eustress" response that is functionally opposed to its well described involvement
191 in pro-inflammatory pathways.

References and Notes

1. J. Grootjans, A. Kaser, R. J. Kaufman, R. S. Blumberg, The unfolded protein response in immunity and inflammation. *Nat Rev Immunol* **16**, 469-484 (2016).
2. S. Bogaert *et al.*, Involvement of endoplasmic reticulum stress in inflammatory bowel disease: a different implication for colonic and ileal disease? *PLoS One* **6**, e25589 (2011).
3. A. Kaser *et al.*, XBP1 links ER stress to intestinal inflammation and confers genetic risk for human inflammatory bowel disease. *Cell* **134**, 743-756 (2008).
4. X. Treton *et al.*, Altered endoplasmic reticulum stress affects translation in inactive colon tissue from patients with ulcerative colitis. *Gastroenterology* **141**, 1024-1035 (2011).
5. T. E. Adolph *et al.*, Paneth cells as a site of origin for intestinal inflammation. *Nature* **503**, 272-276 (2013).
6. N. W. Palm *et al.*, Immunoglobulin A coating identifies colitogenic bacteria in inflammatory bowel disease. *Cell* **158**, 1000-1010 (2014).
7. O. Pabst, New concepts in the generation and functions of IgA. *Nat Rev Immunol* **12**, 821-832 (2012).
8. C. Gutzeit, G. Magri, A. Cerutti, Intestinal IgA production and its role in host-microbe interaction. *Immunol Rev* **260**, 76-85 (2014).
9. A. Kaser, R. S. Blumberg, Paneth cells and inflammation dance together in Crohn's disease. *Cell Res* **18**, 1160-1162 (2008).
10. A. Bitton *et al.*, Clinical, biological, and histologic parameters as predictors of relapse in ulcerative colitis. *Gastroenterology* **120**, 13-20 (2001).
11. M. Tschurtschenthaler *et al.*, Defective ATG16L1-mediated removal of IRE1alpha drives Crohn's disease-like ileitis. *J Exp Med* **214**, 401-422 (2017).
12. S. Luo, C. Mao, B. Lee, A. S. Lee, GRP78/BiP is required for cell proliferation and protecting the inner cell mass from apoptosis during early mouse embryonic development. *Molecular and cellular biology* **26**, 5688-5697 (2006).
13. S. S. Cao *et al.*, The Unfolded Protein Response and Chemical Chaperones Reduce Protein Misfolding and Colitis in Mice. *Gastroenterology*, (2013).
14. L. Mellander, J. Bjorkander, B. Carlsson, L. A. Hanson, Secretory antibodies in IgA-deficient and immunosuppressed individuals. *J Clin Immunol* **6**, 284-291 (1986).
15. J. Fadlallah *et al.*, Microbial ecology perturbation in human IgA deficiency. *Sci Transl Med* **10**, (2018).
16. G. Magri *et al.*, Human Secretory IgM Emerges from Plasma Cells Clonally Related to Gut Memory B Cells and Targets Highly Diverse Commensals. *Immunity* **47**, 118-134 e118 (2017).
17. C. Mauri, M. Menon, Human regulatory B cells in health and disease: therapeutic potential. *J Clin Invest* **127**, 772-779 (2017).
18. F. E. Johansen *et al.*, Absence of epithelial immunoglobulin A transport, with increased mucosal leakiness, in polymeric immunoglobulin receptor/secretory component-deficient mice. *J Exp Med* **190**, 915-922 (1999).

19. A. J. Macpherson *et al.*, A primitive T cell-independent mechanism of intestinal mucosal IgA responses to commensal bacteria. *Science* **288**, 2222-2226 (2000).
20. A. J. Macpherson, K. D. McCoy, F. E. Johansen, P. Brandtzaeg, The immune geography of IgA induction and function. *Mucosal immunology* **1**, 11-22 (2008).
21. H. Yoshida *et al.*, IL-7 receptor alpha+ CD3(-) cells in the embryonic intestine induces the organizing center of Peyer's patches. *Int Immunol* **11**, 643-655 (1999).
22. N. Baumgarth, The double life of a B-1 cell: self-reactivity selects for protective effector functions. *Nat Rev Immunol* **11**, 34-46 (2011).
23. J. J. Bunker *et al.*, Innate and Adaptive Humoral Responses Coat Distinct Commensal Bacteria with Immunoglobulin A. *Immunity* **43**, 541-553 (2015).
24. A. Cerutti, The regulation of IgA class switching. *Nat Rev Immunol* **8**, 421-434 (2008).
25. J. J. Bunker *et al.*, Natural polyreactive IgA antibodies coat the intestinal microbiota. *Science* **358**, (2017).
26. I. M. de Alboran *et al.*, Analysis of C-MYC function in normal cells via conditional gene-targeted mutation. *Immunity* **14**, 45-55 (2001).
27. J. J. Deuring *et al.*, Genomic ATG16L1 risk allele-restricted Paneth cell ER stress in quiescent Crohn's disease. *Gut* **63**, 1081-1091 (2013).
28. G. R. Harriman *et al.*, Targeted deletion of the IgA constant region in mice leads to IgA deficiency with alterations in expression of other Ig isotypes. *J Immunol* **162**, 2521-2529 (1999).
29. E. W. Rogier *et al.*, Secretory antibodies in breast milk promote long-term intestinal homeostasis by regulating the gut microbiota and host gene expression. *Proc Natl Acad Sci U S A* **111**, 3074-3079 (2014).
30. F. el Marjou *et al.*, Tissue-specific and inducible Cre-mediated recombination in the gut epithelium. *Genesis* **39**, 186-193 (2004).
31. A. Ray, B. N. Dittel, Isolation of mouse peritoneal cavity cells. *J Vis Exp*, (2010).
32. S. S. Cao *et al.*, The unfolded protein response and chemical chaperones reduce protein misfolding and colitis in mice. *Gastroenterology* **144**, 989-1000 e1006 (2013).
33. M. A. Koch *et al.*, Maternal IgG and IgA Antibodies Dampen Mucosal T Helper Cell Responses in Early Life. *Cell* **165**, 827-841 (2016).
34. K. Moor *et al.*, Analysis of bacterial-surface-specific antibodies in body fluids using bacterial flow cytometry. *Nat Protoc* **11**, 1531-1553 (2016).
35. H. Wardemann *et al.*, Predominant autoantibody production by early human B cell precursors. *Science* **301**, 1374-1377 (2003).
36. P. Kamran *et al.*, Parabiosis in mice: a detailed protocol. *J Vis Exp*, (2013).
37. K. J. Livak, T. D. Schmittgen, Analysis of relative gene expression data using real-time quantitative PCR and the 2(-Delta Delta C(T)) Method. *Methods* **25**, 402-408 (2001).
38. A. Kaser *et al.*, XBP1 links ER stress to intestinal inflammation and confers genetic risk for human inflammatory bowel disease. *Cell* **134**, 743-756 (2008).

39. A. Butler, P. Hoffman, P. Smibert, E. Papalexi, R. Satija, Integrating single-cell transcriptomic data across different conditions, technologies, and species. *Nat Biotechnol* **36**, 411-420 (2018).
40. A. Dobin *et al.*, STAR: ultrafast universal RNA-seq aligner. *Bioinformatics* **29**, 15-21 (2013).
41. M. I. Love, W. Huber, S. Anders, Moderated estimation of fold change and dispersion for RNA-seq data with DESeq2. *Genome Biol* **15**, 550 (2014).
42. A. Subramanian *et al.*, Gene set enrichment analysis: a knowledge-based approach for interpreting genome-wide expression profiles. *Proc Natl Acad Sci U S A* **102**, 15545-15550 (2005).
43. A. Liberzon *et al.*, Molecular signatures database (MSigDB) 3.0. *Bioinformatics* **27**, 1739-1740 (2011).
44. A. Liberzon *et al.*, The Molecular Signatures Database (MSigDB) hallmark gene set collection. *Cell Syst* **1**, 417-425 (2015).
45. D. A. Bolotin *et al.*, MiXCR: software for comprehensive adaptive immunity profiling. *Nat Methods* **12**, 380-381 (2015).
46. V. Greiff *et al.*, Quantitative assessment of the robustness of next-generation sequencing of antibody variable gene repertoires from immunized mice. *BMC Immunol* **15**, 40 (2014).
47. M. P. Lefranc *et al.*, IMGT, the international ImMunoGeneTics database. *Nucleic Acids Res* **27**, 209-212 (1999).
48. M. Shugay *et al.*, VDJtools: Unifying Post-analysis of T Cell Receptor Repertoires. *PLoS Comput Biol* **11**, e1004503 (2015).
49. T. Joeris, K. Muller-Luda, W. W. Agace, A. M. Mowat, Diversity and functions of intestinal mononuclear phagocytes. *Mucosal Immunol* **10**, 845-864 (2017).

Acknowledgements The authors would like to thank Ken Cadwell (NYU), Tsutomu Chiba (Kyoto University) and Jiri Mestecky (University of Alabama) for useful discussions.

Funding: This work was supported by NIH grants DK044319, DK051362, DK053056, DK088199, the Harvard Digestive Diseases Center (HDDC) DK034854 (R.S.B.); the Wellcome Trust Senior Investigator Award 106260/Z/14/Z, Evelyn Trust 13/27, the HORIZON2020/European Research Council Consolidator Grant (648889, A.K.); the National Institute for Health Research Cambridge BRC Cell Phenotyping Hub (A.K.); Rubicon grant 825.13.012, Netherlands Organization for Scientific Research (J.G.); JSPS KAKENHI grant number 2689323 and 16K19162, Japan Foundation for Applied Enzymology (S.H.); R01AI24998 and R21AI117220 (M.E.C); Deutsche Forschungsgemeinschaft grant KR 4749/1-1 (N.K.) R01 CA238039 (K.W.W.) and Cluster Inflammation at Interfaces ExC306 and BMBF SysINFLAME CP4 to P.R. Pediatric Scientist Development Program K12-HD000850 (J.D.M.). The Howard Hughes Medical Institute supports RAF.

Author contributions: JG, NK, SH, and RSB conceived, designed and interpreted the experiments. JG, NK, SH, JDM, TH, SS, TG, HL, JPL, SGV, SS, AL, YS, JD, GMF, NWP, and MRZ carried out the experiments. JNG, PR, RAF, KDM, AJM, and AK aided with the interpretation of the data. JG, NK, and RSB wrote the manuscript. All authors were involved in critical revision of the manuscript for important intellectual content.

Competing interests: K.W.W. serves on the scientific advisory board of TCR2 Therapeutics, T-Scan Therapeutics and Nextechinvest and receives sponsored research funding from Astellas Pharma, Bristol-Myers Squibb and Novartis.

Data and materials availability: Processed and raw data of the high-throughput sequencing experiments can be downloaded from NCBI Gene Expression Omnibus (GSE124561,

GSE124562). All other data needed to evaluate the conclusions in this paper are present either in the main text or the Supplementary Materials.

Supplementary Materials:

Materials and Methods

Figures S1-S19

Tables S1-S2

References (*28-49*)

Figure Legends

Fig. 1. Intestinal epithelial ER stress induces a protective IgA response. (A) Absolute counts of SI LP IgA$^+$ plasma cells in *Xbp1*$^{\Delta IEC}$ mice and *Xbp1*$^{fl/fl}$ controls at 10 weeks of age ($n = 7–8$). **(B)** Ileal tissue IgA normalized by total soluble tissue protein ($n = 8–10$). **(C)** IgA concentration in SI washes ($n = 6–10$). **(D)** Circulating IgA concentration ($n = 6–10$ for each age). **(E** and **F)** Representative images (E) and quantification (F) of LP IgA$^+$ cells (brown) along ≥ 50 ileal crypt–villus axes ($n = 6–7$). Magnified area depicts basal plasmacytosis. **(G)** Representative images and quantification of SI LP IgA$^+$ cells (red) in *Grp78*$^{T\text{-}\Delta IEC}$ mice and *Grp78*$^{fl/fl}$ controls after 3 days of tamoxifen treatment ($n = 4$). **(H** and **I)** Absolute counts of SI LP IgA$^+$ plasma cells (H) and circulating IgA concentrations (I) of the indicated genotypes, treated with either TUDCA (2 mg/ml) in the drinking water or plain water (control) for two weeks ($n = 7–8$). **(J** and **K)** Enteritis scores of ileal (J) and jejunal (K) sections of indicated genotypes. ($n = 4–26$). **(L)** Representative plots, frequencies, and absolute counts of SI LP IgM$^+$ plasma cells (gated on CD45$^+$CD3$^-$ lymphocytes) of the indicated genotypes ($n = 3–14$). **(M** to **O)** Absolute flow cytometric counts of SI LP IgA$^+$ plasma cells (M), representative images and quantification of IgA$^+$ cells in ileal sections (N) and enteritis scores (O) of *Pigr*$^{-/-}$ *Xbp1*$^{\Delta IEC}$ mice and *Pigr*$^{-/-}$ *Xbp1*$^{fl/fl}$ controls ($n = 9–18$). **(P)** Frequencies of IgA-coated fecal bacteria from the indicated genotypes as determined by flow cytometry ($n = 2–20$). B6, C57BL/6J background. Scale bars, 100 μm (low magnification) or 20 μm (insets). Symbols represent individual animals.

Bars represent arithmetic means (B, D, F, G, I, N and P), medians (J, K and O)2 or geometric means (A, C, H, L and M). Error bars indicate standard error of mean. Data are representative of three (A and B) independent experiments or were compiled from two (M) or three (L and P) experiments. *P*-values were calculated by unpaired Student's *t*-test (A to D, F, G, L to N, P), Kruskal–Wallis test with Dunn's post test (J and K), Mann–Whitney *U* test (O), or two-way ANOVA with Fishers LSD method and two-stage step-up method of Benjamini, Krieger, and Yekutieli to control the false discovery rate (H and I). $*P < 0.05$, $**P < 0.01$, $***P < 0.001$.

Fig. 2. ER stress-induced IgA is PP- and T cell-independent and involves recruitment of peritoneal B1b cells by a transmissible factor. (A) Representative plots and percentages of germinal center (GC) B cells (gated on $CD19^+$ lymphocytes) in MLN and PP of $Xbp1^{\Delta IEC}$ mice and $Xbp1^{fl/fl}$ controls ($n = 4–7$). **(B)** Representative plots and percentages of MLN and PP follicular T helper cells (Tfh, gated on $CD3^+CD4^+$ lymphocytes, $n = 4–6$). **(C)** Absolute counts of SI LP IgA^+ plasma cells in $TCR\beta^{-/-}Xbp1^{\Delta IEC}$ mice and $TCR\beta^{-/-}Xbp1^{fl/fl}$ controls ($n = 8–9$). **(D)** Absolute counts of SI LP IgA^+ plasma cells in PP-deficient $Xbp1^{\Delta IEC}$ mice and $Xbp1^{fl/fl}$ controls (n = 6–8). **(E** and **F)** Representative plots, percentages, and absolute counts of peritoneal B1a and B1b cells in $Xbp1^{\Delta IEC}$ mice and $Xbp1^{fl/fl}$ controls ($n = 5–7$). **(G)** Schematic representation of the parabiosis experiment ($n = 7–8$ pairs per genotype). **(H)** Frequencies of $CD45.1^+$ circulating lymphocytes and $CD45.1^+$ peritoneal B1 cells 3 weeks after parabiotic surgery. Dotted line indicates 50% chimerism. **(I)** Absolute numbers of $CD45.1^+$ B1b cells in peritoneal cavities of CD45.1 animals, conjoined with $Xbp1^{fl/fl}$ and $Xbp1^{\Delta IEC}$ mice, respectively. **(J** and **K)** Absolute numbers of SI LP $CD45.1^+IgA^+$ plasma cells in parabiotic $Xbp1^{fl/fl}$ and $Xbp1^{\Delta IEC}$ mice (J) and in CD45.1 parabionts, conjoined with $Xbp1^{fl/fl}$ and $Xbp1^{\Delta IEC}$ mice,

respectively (K). Symbols represent individual animals. Bars represent arithmetic means (A, B, E, and H) or geometric means (C, D, F, I–K). Data are representative of three experiments (E and F) or were pooled from two experiments (C, D, G–K). *P*-values were calculated by unpaired Student's *t*-test. *$P < 0.05$, **$P < 0.01$, ***$P < 0.001$.

Fig. 3. Epithelial ER stress-derived IgA is microbiota- and inflammation-independent and polyreactive in nature. (A) Absolute counts of SI LP IgA^+ plasma cells in germ-free (GF) *Xbp1*$^{\Delta IEC}$ mice and *Xbp1*$^{fl/fl}$ controls ($n = 7–8$). **(B)** Representative images and quantification of LP IgA^+ cells (green) along ≥ 50 ileal crypt-villus axes ($n = 3–6$). Nuclei are counterstained with DAPI (blue). Arrows indicate basal plasmacytosis. **(C** and **D)** Frequencies (% of $CD19^+CD23^-CD43^+$ cells) and absolute flow cytometric counts of peritoneal B1a and B1b cells (n = 7–8). **(E)** Representative plots (gated on $CD5^-CD19^+CD43^+$ lymphocytes) and frequencies of IgA^+ B1b-derived cells in SI LP of GF *Xbp1*$^{\Delta IEC}$ mice and GF *Xbp1*$^{fl/fl}$ controls (n = 7–8). **(F)** *t*-SNE plot depicting unsupervised clustering of single-cell transcriptomes ($n = 11{,}104$ cells) from peritoneal lavages of *Xbp1*$^{\Delta IEC}$ mice and *Xbp1*$^{fl/fl}$ controls (aligned data sets). **(G)** Expression levels of canonical markers for macrophages (*Csf1r*), B cells (*Cd79a*), T cells (*Cd3e*), and peritoneal dendritic cells (*Cd209a*) in *t*-SNE plot. **(H)** *t*-SNE plot as in (F) with cells colored by genotype. Bar graph depicts numbers of cells within each cluster by genotype. **(I)** Volcano plot showing $\log_2$-transformed fold-change (log2FC) of gene expression in B1b cells from GF *Xbp1*$^{\Delta IEC}$ mice compared to GF *Xbp1*$^{fl/fl}$ controls ($n = 5–7$). Differentially expressed genes (log2FC ≥ 1 or ≤ −1, FDR < 0.05) are highlighted in blue. FDR values < 10^{-5} are plotted at 10^{-5} (triangles). **(J)** GSEA enrichment plots for selected gene sets. NES, normalized enrichment score. **(K)** Circulating IgA concentrations in GF *Xbp1*$^{\Delta IEC}$ mice and *Xbp1*$^{fl/fl}$ controls ($n = 12–13$).

(L) Representative plots (gated on $SYBR^{hi}$ events) and frequencies of IgA coating on fecal bacteria from μMT mice that were incubated with sera from GF *Xbp1*$^{\Delta IEC}$ mice or *Xbp1*$^{fl/fl}$ controls ($n = 4–5$). **(M)** Polyreactivity ELISA OD_{650} values of serum IgA from GF *Xbp1*$^{\Delta IEC}$ mice or *Xbp1*$^{fl/fl}$ controls (n = 5–6) against the indicated antigens. Scale bar, 100 μm. Symbols or lines represent individual animals. Bars represent arithmetic means (B, C and E) or geometric means (A, D and K). Data are representative of at least two independent experiments (B to D, L and M) or were pooled from two experiments (A, E and K). *P*-values were calculated by unpaired Student's *t*-test. $*P < 0.05$, $**P < 0.01$, $***P < 0.001$.

Fig. 4. Defective ATG16L1-dependent autophagy results in a peritoneal B1b response in mice, and IgA induction in both mice and humans. (A) Representative images and quantification of LP IgA^+ cells (brown) along ≥ 50 ileal crypt-villus axes of *Atg16l1*$^{\Delta IEC}$ mice and *Atg16l1*$^{fl/fl}$ controls ($n = 8$). **(B)** Absolute counts of peritoneal B1a and B1b cells in *Atg16l1*$^{\Delta IEC}$ mice and *Atg16l1*$^{fl/fl}$ controls ($n = 7–12$). **(C)** Representative images and quantification of IgA^+ cells (brown) in ileal biopsies of healthy human subjects, shown by ATG16L1 genotype ($n = 8–16$). Scale bar, 100 μm. Symbols represent individual animals or human subjects. Bars represent arithmetic means (A and C) or geometric means (B). Data in (B) were pooled from two experiments. *P*-values were calculated by unpaired Student's *t*-test (A and B) or one-way ANOVA with Holm–Šídák test (C). $*P < 0.05$, $**P < 0.01$, $***P < 0.001$.

Science
AAAS

Supplementary Materials for

Epithelial endoplasmic reticulum stress orchestrates a protective IgA response

Joep Grootjans†, Niklas Krupka†, Shuhei Hosomi†, Juan D. Matute, Thomas Hanley, Svetlana Saveljeva, Thomas Gensollen, Jarom Heijmans, Hai Li, Julien P. Limenitakis, Stephanie C. Ganal-Vonarburg, Shengbao Suo, Adrienne M. Luoma, Yosuke Shimodaira, Jinzhi Duan, David Q. Shih, Margaret E. Conner, Jonathan N. Glickman, Gwenny M. Fuhler, Noah W. Palm, Marcel R. de Zoete, C. Janneke van der Woude, Guo-Cheng Yuan, Kai W. Wucherpfennig, Stephan R. Targan, Philip Rosenstiel, Richard A. Flavell, Kathy D. McCoy, Andrew J. Macpherson, Arthur Kaser, Richard S. Blumberg*

† These authors contributed equally to this work.
* Correspondence to rblumberg@bwh.harvard.edu

This PDF file includes:

Materials and Methods

Mice

C57BL/6J *Villin-cre*$^{+}$*;Xbp1*$^{fl/fl}$ (*Xbp1*$^{\Delta IEC}$), *Villin-cre*$^{+}$*;Ern1*$^{fl/fl}$*;Xbp1*$^{fl/fl}$ (*Ern1/Xbp1*$^{\Delta IEC}$) and *Villin-cre*$^{+}$*;Atg16l1*$^{fl/fl}$ *(Atg16l1*$^{\Delta IEC}$*)* mice were obtained as described before (*5*). C57BL/6J *TCRβ*$^{-/-}$ mice (B6.129P2-*Tcrb*^{tm1Mom}/J), *μMT* mice (B6.129S2-*Ighm*^{tm1Cgn}/J), CD45.1 mice (B6.SJL-*Ptprc*^{a}*Pepc*^{b}/BoyJ) and IL-10 reporter mice (Vert-X, B6(Cg)-*Il10*$^{tm1.1Karp}$/J) were purchased from Jackson Laboratories. *Igha*$^{-/-}$ mice (*Igha*^{tm1Grh}) were provided by Dr. M. Conner (*28*), and *Pigr*$^{-/-}$ mice (B6.129P2-*Pigr*^{tm1Fejo}) obtained from Dr. C.S. Kaetzel and Dr. M. Karin (*18, 29*). Mice were analyzed at 10–12 weeks of age unless otherwise indicated. For all conditional knockouts, sex- and age-matched *Villin-cre*$^{-}$ littermates were used as controls. All mice were maintained in a specific pathogen-free environment at Harvard Medical School or at the central biomedical services facility of the University of Cambridge, UK (*Ern1/Xbp1*$^{\Delta IEC}$*, Atg16l1*$^{\Delta IEC}$*)*, according to institutional guidelines and the approval of relevant authorities.

Germ-free C57BL/6 *Villin-cre*$^{+}$*;Xbp1*$^{fl/fl}$ (GF *Xbp1*$^{\Delta IEC}$) mice and their littermate controls *Villin-cre*$^{-}$*;Xbp1*$^{fl/fl}$ mice were obtained as described before (*5*), and housed at the Harvard gnotobiotic facility under strict germ-free conditions.

Experiments with the C57BL/6 *Villin-creERT2*$^{+}$*;Grp78*$^{fl/fl}$ (*Grp78*$^{T\text{-}\Delta IEC}$) mice were performed in the Academic Medical Center Animal Research Institute in accordance with local guidelines. *Villin-creERT2* mice have been described previously (*30*). *Grp78*$^{fl/fl}$ mice (*Hspa5*^{tm1Alee}) were kindly provided by the Lee lab (*12*). For Cre-ER^{T2}-mediated recombination, mice were administered three intraperitoneal injections of 50 mg/kg tamoxifen (Sigma-Aldrich, 10 mg/ml in corn oil) during three consecutive days and were sacrificed 24 hours thereafter.

Cell isolation

Lamina propria: 10 cm of distal small intestine was excised and mesenterium, fat, intestinal contents and Peyer's Patches were carefully removed. Intestines were opened longitudinally and cut into 1–2 cm pieces. Samples were then placed into a 50-ml tube with 20 ml of HBSS 3 mM EDTA (Fisher) and incubated for 10 minutes at 37 °C and 250 rpm on a shaking incubator (New Brunswick Scientific I2500). The supernatant, containing mucus and epithelial debris, was discarded and the wash steps repeated twice for another 10 and 20 minutes, respectively, using fresh HBSS 3 mM EDTA. The tissue pieces were then collected, washed once in HBSS and placed into a new 50-ml tube with 10 ml of RPMI 10% FBS (Atlanta Biologicals), 1.5% HEPES (Corning), antibiotic/antimycotic (Gibco), 1 mg/ml of collagenase VIII, and 50 μg/ml of DNase I (both Sigma). Samples were incubated for 30 minutes at 37 °C and 250 rpm. Supernatant containing isolated cells was then passed through a 100-μm cell strainer, washed with PBS 2% FBS, 2 mM EDTA, passed through a 40-μm cell strainer and washed again.

Peyer's patches and mesenteric lymph nodes (MLNs): Peyer's patches and MLNs were minced and passed through a 70-µm cell strainer with the plunger end of a 1-ml syringe, washed once in PBS 2% FBS, 2 mM EDTA and passed again through a 40-µm cell strainer.
Peritoneal cells: The isolation of peritoneal cavity cells was performed as described previously (*31*). Briefly, the peritoneal lining of a euthanized mouse was exposed by carefully cutting and pulling back the outer skin layer. Then, 5 ml of ice-cold PBS 2% FBS, 2 mM EDTA was injected into the peritoneal cavity using a 27G needle. The peritoneum was gently massaged to dislodge cells and the peritoneal contents collected using a 25G needle. Samples with visible blood contamination were discarded. Peritoneal contents were washed once in PBS 2% FBS, 2 mM EDTA and passed through a 40-µm cell strainer.

Flow cytometry

Single-cell suspensions were incubated with anti-mouse CD16/32 (clone 93, Biolegend) and with Fixable Viability Dye (eBioscience, each 20 minutes at 4 °C) prior to staining. Antibodies used for staining are listed in Table S1. Cells were incubated in antibody cocktail in PBS 2% FBS, 2 mM EDTA for 30 minutes at 4 °C. When required, intracellular staining was performed using a FOXP3 staining kit (eBioscience). After staining, cells were washed 2–3 times in PBS 2% FBS, 2 mM EDTA and acquired on a MACSQuant Analyzer (Miltenyi Biotec), Cytoflex S (Beckman Coulter) or LSRFortessa (BD Biosciences). Data were analyzed using FlowJo software v10 (TreeStar).

Immunoglobulin ELISAs

Intestinal washes were obtained by gently flushing the whole small intestine with 5 ml of wash buffer (PBS, 0.05 M EDTA, Complete Mini protease inhibitors, Roche) into a petri dish on ice. Debris was removed by centrifuging at 4,000 rpm at 4 °C for 15 minutes, after which the supernatant was collected and stored at −80 °C until required. Tissue homogenates were obtained by mechanical disruption of tissue (40 mg/ml) in PBS containing protease inhibitors (Complete Mini, Roche). Serum and plasma were obtained from tail snip blood sample collections. For normalization, total protein concentration of the soluble fraction was measured by BCA assay (Thermo Scientific).
Immunoglobulin levels were measured by standard sandwich ELISA (antibodies listed in Table S2). Briefly, ELISA plates (Corning) were coated with capture antibodies and washed extensively using an ELISA plate washer (Biotek ELx 405). Plates were then blocked with PBS 1%–2% BSA (Fisher) for 1–2 hours at room temperature and washed again. Samples and standards were added to wells and incubated for 1–2 hours at room temperature. All samples and serially diluted standards were run in duplicate. Plates were then washed and incubated with HRP-conjugated detection antibodies for one hour at room temperature. After washing again, 3,3',5,5'-tetramethylbenzidine (TMB) substrate (KPL) was added and incubated for 10–15 minutes at room temperature. The reaction was stopped by adding 0.18 M H_2SO_4 and absorbance at 450 nm was read on a microplate

reader (VersaMax, Molecular Devices). Analyte concentrations were determined by comparison with standards using a four-parameter logistic regression.

TUDCA treatment of animals

Tauroursodeoxycholic acid (TUDCA, Cayman Chemical) was dissolved in autoclaved tap water at a concentration of 2 mg/ml as described previously (*32*) and provided as drinking water for 14 days. The animals were monitored daily, and drinking water was replaced every 48 hours. Water intake measurements showed that both TUDCA-treated and control mice, which received autoclaved tap water, consumed an average of 4 ml/d (400 mg/kg body weight assuming an average body weight of 20 g). Blood samples were collected by tail snips (baseline) or cardiac puncture (post-treatment). The post-treatment sample of one animal could not be obtained for technical reasons.

Intestinal explant culture

For intestinal explant culture, two whole-layer punches cut by Tru-Punch™ Sterile Disposable Biopsy Punch 6 mm (Sklar) were incubated in 24-well tissue culture plates containing 500 µl of RPMI 2% FBS (Atlanta Biologicals), 1% HEPES (Corning), and antibiotic/antimycotic (Gibco) at 37 °C and 5% CO_2 for 24 hours. The supernatants were analyzed for IL-10 by Cytometric Bead Array (CBA, Mouse Th1/Th2/Th17 Cytokine Kit, BD Biosciences) and for TSLP by Mouse TSLP Quantikine ELISA Kit (R&D Systems) according to the manufacturer's instructions.

H&E staining and histology

Small-intestinal tissues from mice were isolated using standard techniques and formalin-fixed, paraffin-embedded tissue was stained with hematoxylin and eosin (H&E) as described (*5*). A semi-quantitative composite scoring system was used for the assessment of spontaneous intestinal inflammation, calculated as a sum of four histological subscores: mononuclear cell infiltration (0: absent; normal sparse lymphocytic infiltration, 1: mild; diffuse increase in lamina propria, 2: moderate; lamina propria increased with basal localization aggregates displacing crypts, 3: severe; lamina propria with submucosal infiltration), crypt hyperplasia (0: absent, 1: mild, 2: moderate, 3: severe), epithelial injury/erosion (0: absent, 1: mild; crypt dropout or surface epithelial damage without frank erosion or ulceration, 2: moderate; focal ulceration, 3: severe; multifocal or extensive ulceration) and polymorphonuclear cell infiltration (0: absent, 1: mild; lamina propria only, 2: moderate; lamina propria infiltration with cryptitis or crypt abscesses, 3: severe; sheet-like or submucosal infiltration). Scores were multiplied by a factor based on the extent of the inflammation. Extent factor was derived according to the fraction of bowel length involved by inflammation: 1, $<10\%$; 2, 10%–25%; 3, 25%–50%; and 4, $>50\%$. The score was assessed by an expert gastrointestinal pathologist (J.N.G.) who was blinded to the genotype and experimental conditions of the samples.

Immunohistochemistry and immunofluorescence

Intestinal sections were deparaffinized in xylene and rehydrated in graded ethanol to distilled water. For immunohistochemistry, endogenous peroxidase activity was blocked using 3% hydrogen peroxide in distilled water for 10 minutes. After heat-mediated antigen retrieval in 10 mM citrate buffer (pH 6.0), non-specific antibody binding sites were blocked (Animal-Free Blocking Solution, Cell Signaling Technologies), and sections were incubated overnight at 4 °C with 0.5 µg/ml rabbit anti-mouse IgA antibody (NB7506, Novus Biologicals), 1:125 rabbit anti-Cre Recombinase (D7L7L, Cell Signaling Technology) or 1:1,600 rabbit anti-human/mouse BiP (C50B12, Cell Signaling Technology), respectively. After thorough washing of the sections, an HRP-conjugated anti-rabbit polymer (SignalStain Boost IHC Detection Reagent, Cell Signaling Technologies) was applied and targets visualized by 3,3′-diaminobenzidine-tetrahydrochloride-dihydrate (DAB, Cell Signaling Technologies). Sections were counterstained with hematoxylin. For immunofluorescence, targets were visualized using 2 µg/ml Alexa Fluor 488–conjugated donkey anti-rabbit IgG (A21206, Invitrogen) and nuclei counter-stained with 4′,6-diamidino-2-phenylindole (DAPI, Invitrogen). No staining was detected in slides incubated without primary antibodies or with an isotype control. For IgA quantification, IgA^+ cells were counted along ≥50 crypt/villus axes. For epithelial GRP78 (BiP) quantification, the mean staining intensity of epithelial layers from three random fields per sample (200-fold magnification) was calculated using ImageJ.

Microbiota flow cytometry

Bacterial flow was performed as described previously (*6, 33*). Briefly, fresh fecal pellets were gently homogenized in 500 µl of staining buffer (PBS, 1% w/v BSA) and centrifuged at 50 × *g* for 15 minutes at 4 °C to remove large non-bacterial particles. The supernatant (100 µl) was transferred to a fresh tube, washed with 1 ml staining buffer, centrifuged at 8,000 × *g* for 5 minutes and resuspended again in 1 ml staining buffer. IgA staining was performed by incubating 25 µl of the resuspended bacteria with 2.5 µg/ml PE-conjugated anti-IgA antibody (mA-6E1, eBioscience) for 30 minutes on ice. Samples were washed two times and resuspended in staining buffer with SYBR Green (Thermo Fisher) before flow cytometric analysis (Cytoflex S, Beckman Coulter). Bacteria were identified as $SYBR^{hi}$ events as described previously (*33*).

IgA-seq

Samples were prepared as described above for microbiota flow cytometry. Following staining of the bacteria with 16 µg/ml PE-conjugated anti-IgA antibody (mA-6E1, eBioscience) for 30 minutes on ice, samples were washed three times. Then, 2 million IgA^+ and 2 million IgA^- bacteria were isolated via FACS (FACSAria; BD Biosciences). Isolated bacteria were pelleted (10,000 × *g*, 5 minutes, 4 °C) and frozen along with the pre-sort samples. 16S rRNA gene sequencing was performed as described previously (*6*).

Flow cytometric analysis of serum IgA bacterial reactivity

Antibacterial reactivity of serum IgA was assessed as described previously (*34*). Briefly, sera were heat-inactivated at 56 °C for 30 minutes, centrifuged at 16,000 × *g* for 5 minutes and passed through a 0.22-μm spin filter column. Serially diluted sera (in PBS, 1% w/v BSA) were then incubated with 1.25×10^5 non-IgA-coated bacteria, which were obtained from feces of SPF μMT mice, for 1 hour on ice. IgA staining and cytometric acquisition were performed as described above.

Polyreactivity ELISAs

Polyreactivity of serum IgA was assessed as described previously (*25, 35*). Briefly, high-binding ELISA plates (Corning) were coated overnight with recombinant calf thymus DNA (10 μg/ml, Sigma), human insulin (5 μg/ml, Sigma), keyhole limpet hemocyanin (KLH) (10 μg/ml, Sigma), LPS from *E. coli* (10 μg/ml, Sigma) in bicarbonate buffer or cardiolipin (10 μg/ml, Sigma) in 100% ethanol. Cardiolipin-coated plates were allowed to dry overnight. Plates were washed five times with distilled water using an ELISA plate washer (Biotek ELx 405) and incubated with ELISA buffer (PBS, 1 mM EDTA, 0.05% Tween 20) for 1 hour at room temperature. Plates were washed five times and serially diluted sera (in PBS) were added for 2 hours at room temperature. Plates were washed five times, incubated with HRP-conjugated goat anti-mouse antibody (Bethyl) in ELISA buffer for 1 hour and washed again. ELISA buffer was then added, and plates incubated for 5 minutes at room temperature. Plates were washed again and TMB substrate (KPL) was added. Optical densities at 650 nm were monitored using a microplate reader (VersaMax, Molecular Devices).

Generation of Peyer's patch-deficient animals

Peyer's patch-deficient animals were generated as previously described (*21*). Briefly, mice were mated overnight (day 0). At day 14.5, a single intravenous injection of 3 mg of anti-IL7Rα (clone A7R34, BioxCell) was administered to pregnant females under axenic conditions. This completely abrogated Peyer's patch ontogeny in the pups, which was confirmed macroscopically and microscopically.

Parabiosis experiments

Parabiosis was performed as described previously (*36*). Briefly, co-housed female mice of similar weight and size were anesthetized using an isoflurane vaporizer (4%–5% v/v) connected to a Posi-Seal induction chamber. Anesthesia was maintained throughout the surgical procedure via a nose cone connected to isoflurane (1.5%–2% v/v). For analgesia, carprofen and buprenorphine were administered i.p. at a dose of 10 mg/kg and 0.1 mg/kg respectively. After aseptically preparing the surgical areas (approximately 1 cm above the elbow to 1 cm below the knee), longitudinal skin incisions were performed, and the skin was gently detached from the subcutaneous fascia along

the incision. Olecranons and knee joints were joint using a non-absorbable 3-0 suture and skin connected with a continuous absorbable 5-0 Vicryl suture. Following recovery, analgesics were provided at the previously described dosage every 24 hours for 2 days. Furthermore, antibiotic prophylaxis with sulfamethoxazole/trimethoprim was administered via drinking water (2 mg/ml and 0.4 mg/ml, respectively). Animals were carefully monitored for signs of pain, distress, or infection.

RNA isolation and RT-qPCR

RNA from small-intestinal tissue was extracted and purified using RNeasy Mini Kit (Qiagen), and complementary DNAs (cDNA) were synthesized using SuperScript III reverse transcriptase (Life Technologies). Real-time RT-PCR was performed using LightCycler 480 SYBR Green I Master (Roche) and a CFX96 Real-Time System (Bio-Rad). Values were normalized to *Gapdh* and relative expression calculated using the $2^{-\Delta\Delta CT}$ method (*37*). Primers used for qPCR were as follows:

Gapdh forward: 5′-AGGTCGGTGTGAACGGATTTG-3′,
reverse: 5′-TGTAGACCATGTAGTTGAGGTCA-3′,
Tnfsf13 forward: 5′-GCCAGCCTCATCTCCTTTCTTG-3′,
reverse: 5′-TGGTTGCCACATCACCTCTGTCAC-3′,
Tnfsf13b forward: 5′-CTGTGGTCACTTACTCCAAAGG-3′,
reverse: 5′-GGATCAGATTCAACGGGTCACG-3′,
Ccl25 forward: 5′-TTACCAGCACAGGATCAAATGG-3′,
reverse: 5′-CGGAAGTAGAATCTCACAGCAC-3′,
Ccl28 forward: 5′-AGAGTGAGTTCATGCAGCATC-3′,
reverse: 5′- CTGCTTCAAAGTACGATTGTGC-3′,
Cxcl13 forward: 5′-GGCCACGGTATTCTGGAAGC-3′,
reverse: 5′-GGGCGTAACTTGAATCCGATCTA-3′

Xbp1 splicing assay

Splicing of *Xbp1* was quantified from cDNA of whole-thickness small-intestinal tissue RNA samples as described previously (*38*). Briefly, a region of *Xbp1* including the splicing site was amplified by PCR using the following primers: *Xbp1s* forward: 5′ACACGCTTGGGAATGGACAC-3′, reverse: 5′-CCATGGGAAGATGTTCTGGG-3′. The resulting amplicons of 145 bp (spliced) and 171 bp (unspliced) were resolved on a 2% agarose gel with SYBR Safe DNA Gel Stain (Thermo Fisher) and visualized using an Odyssey Fc Imaging System (LI-COR Biosciences).

Immunoblotting

Proteins for immunoblotting were extracted from small-intestinal tissue by homogenizing samples in immunoprecipitation buffer (20 mM Tris pH 8.0, 150 mM NaCl, 1 mM EDTA and 1% Triton-X) with protease inhibitors (Complete Mini, Roche). Thirty micrograms of soluble protein (as determined by BCA Protein Assay, Thermo Fisher) was electrophoretically separated on a 4%–20% gradient tris/glycine gel (Thermo Fisher) and transferred onto nitrocellulose membranes (Thomas Scientific). Membranes were blocked with TBS-based Odyssey Blocking buffer (LI-COR Biosciences) and incubated at 4 °C overnight in Odyssey Blocking buffer with 0.1% Tween and the following primary antibodies: 1:1,000 rabbit anti-IRE1α (14C10, Cell Signaling Technology), and 1:1,000 chicken anti-beta actin (ab13822, Abcam). After washing, membranes were incubated for 1 hour at room temperature in Odyssey Blocking buffer with 0.1% Tween and 1:15,000 IRDye 800CW goat anti-rabbit IgG and 1:20,000 IRDye 680LT donkey anti-chicken IgG (LI-COR Biosciences). Membranes were visualized using an Odyssey Fc Imaging System (LI-COR Biosciences) and band density quantified using Image Studio Software (LI-COR Biosciences).

TUNEL labeling

Apoptotic cell death was assessed on formalin-fixed, paraffin-embedded small-intestinal tissue sections by TdT-mediated dUTP nick-end labelling (TUNEL) using a TACS 2 TdT DAB In Situ Apoptosis Detection Kit (Trevigen) according to the manufacturer's protocol. Positive controls were obtained by nuclease treatment of sections.

Single-cell RNA-seq

Peritoneal cavity cells of four male, age-matched GF *Xbp1*$^{\Delta IEC}$ mice and four GF *Xbp1*$^{fl/fl}$ littermate controls were isolated by lavage as described previously and equal cell numbers of each animal pooled by genotype. For each pooled sample, 8,700 cells were encapsulated into droplets using Chromium Controller (10x Genomics). Libraries were prepared using Chromium Single Cell 3′ Library Kits v2 (10x Genomics) according to the manufacturer's protocol. Following quality control using a Bioanalyzer 2100 (Agilent), equal quantities of each library were pooled and sequenced over two lanes of a HiSeq 2500 Rapid Run Flow Cell (Illumina) using custom parameters: Read 1, 26 cycles; i7, 8 cycles; i5, 0 cycles; Read 2, 98 cycles.

Raw scRNA-seq data were processed using the Cell Ranger Pipeline (v2.2.0, 10x Genomics), obtaining 6,076 and 6,028 single cells from GF *Xbp1*$^{\Delta IEC}$ and GF *Xbp1*$^{fl/fl}$ mice, respectively, with an average of ~27,000 reads per cell. Both libraries were aggregated using the Cell Ranger "aggr" function. Then, DoubletFinder (https://doi.org/10.1101/352484) was used to filter potential doublets. Finally, the UMI-collapsed count matrix of the remaining 11,104 single cells was fed to Seurat (v2.3.0) to perform clustering analysis and identify potential marker genes (*39*). Briefly, we only included cells with ≥200 detected genes and genes detected in ≥12 cells, log-normalized

the expression data and identified highly variable genes. Finally, shared nearest neighbor (SNN) was applied for clustering and *t*-distributed stochastic neighbor embedding (*t*-SNE) was used to visualize the single cell transcriptional profile in 2D space.

RNA-seq

For each sample, 6,000 peritoneal B1b cells ($CD19^+CD23^-CD5^-CD3^-F4/80^-$) were isolated by FACS with a confirmed post-sort purity of > 90%. RNA was isolated using the RNeasy Plus Micro Kit (Qiagen) and concentrations determined using a Bioanalyzer 2100 (Agilent). RIN scores of all samples were ≥ 8.9. Library preparation was performed using SMART-Seq v4 Ultra Low Input RNA Kit (Takara). Pooled libraries were sequenced by Illumina NextSeq 500 in single-end mode using a 75-cycle high output kit. The number and quality of demultiplexed reads were assayed using FastQC v0.11.5 (https://www.bioinformatics.babraham.ac.uk/projects/fastqc). Adaptors were trimmed using TrimGalore! v0.4.4 (https://www.bioinformatics.babraham.ac.uk/projects/trim_galore). Reads were mapped to the NCBI GRCm38.p5 mouse genome using STAR v2.5.2b (*40*) with default settings. Reads per gene were counted using STAR's *"--quantMode GeneCounts"* function with the Ensembl annotation release 91. Differential expression was assessed using DESeq2 v1.18.1 with default parameters (*41*). Moderated log fold changes, obtained by the DEseq2 *lfcshrink* function, were used for visualization.

For gene set enrichment analysis (GSEA) (*42*), a pre-ranked gene list was generated using the following formula:

$$\text{Rank metric} = |\log_2 FC|/\log_2 FC \times -\log_{10}(P\text{-value})$$

GSEA was performed using GSEA v3.0 software (Broad Institute) in pre-ranked mode with 1,000 permutations and classic enrichment score calculation against MSigDB v6.1 collections H and C5BP (*43, 44*).

Human IgA quantification

Previously collected tissue was used for analysis (*11*). Briefly, after obtaining written informed consent, intestinal biopsies from the terminal ileum of 43 healthy controls were collected during colonoscopy. Formalin-fixed, paraffin-embedded sections were stained by immunohistochemistry as described above, using mouse anti-human IgA antibody (NCL-L-IgA, 1:400, Leica Biosystems) and HRP-conjugated horse anti-mouse IgG polymer (Vector Laboratories). Nine samples had low tissue quality and were excluded before quantification. IgA^+ cells were quantified within three randomly selected high-power fields per sample in a blinded fashion.

Genotyping for ATG16L1 (T300A) SNP (rs2241880) was performed as described previously (*11*). Briefly, DNA from EDTA blood samples was extracted (Wizard Genomic DNA purification kit; Promega) and a 330-bp fragment containing the ATG16L1 (T300A) SNP amplified by High-Fidelity PCR (Phusion; Thermo Fisher Scientific) using forward primer 5′-TTGGAGTCCACAGGTTAG-3′

and reverse primer 5′-CAGTAGCTGGTACCCTCACTTC-3′ (*11*). PCR products were run on a 1% agarose gel and the appropriate fragment cut and purified (QIAQuick gel extraction kit, Qiagen). Sanger sequencing of the amplicons was then performed using the forward primer. All protocols were approved by Cambridgeshire 4 Research Ethics Committee (reference 03/5/012). Patient characteristics were reported previously (*11*).

IgA repertoire sequencing

Illumina-based antibody repertoire sequencing library pools were sequenced on the Illumina MiSeq platform (2 × 250 cycles, paired-end) with 10% PhiX control library. Mean base-call quality of all samples was in the range of Phred score 30. The resulting FASTQ files were preprocessed (VDJ alignment, clonotyping) using the MiXCR software package (clonotype formation by CDR3 amino acid region, annotated using C57BL/6J germline gene data, https://github.com/milaboratory/mixcr) (*45*). Error correction was performed by combining previously published bioinformatics workflows (reduction of artificial diversity by singleton exclusion and CDR3 length restriction) with the MiXCR platform (*46*). PCR and sequencing errors were corrected using the built-in function of MiXCR for clonotyping by multilayer clustering (assembly of consensus CDR3 sequences having homologous and identical CDR3s).

For all analyses, clones were defined by 100% amino acid sequence identity of CDR3 regions. CDR3 regions were defined by MiXCR according to the nomenclature of the Immunogenetics database (IMGT) (*47*). MIXCR output files were further processed in VDJtools post-analysis framework (https://github.com/mikessh/vdjtools) (*48*). Further filtering was applied in order to keep only in-frame, productive sequences. Basic statistic segment usage was calculated, and weighted variable usage profiles were hierarchically clustered and visualized as a heatmap. Repertoire overlap was measured by calculating the geometric mean of relative overlap frequencies between variable segment usage profiles or CDR3 usage. The relative overlap similarity was represented as hierarchical clustering or multi-dimensional scaling (MDS) plot.

Statistical analysis

Statistical significance was determined as indicated in the figure legends. Differences were considered significant at $P < 0.05$. Data were analyzed using GraphPad Prism v7 (GraphPad Software).

Supplementary Figures

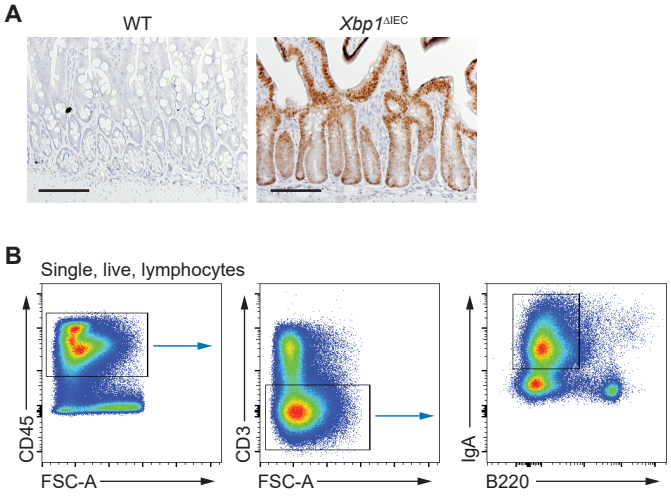

Fig. S1. IEC-restricted expression of Cre recombinase in *Xbp1*$^{\Delta IEC}$ mice and gating strategy for small-intestinal LP IgA^{+} plasma cells. (A) IHC for Cre recombinase (brown) in ileal tissue of wild-type C57BL/6J (WT) and *Xbp1*$^{\Delta IEC}$ mice ($n=2$, one experiment). **(B)** Gating strategy. Plots are representative of multiple independent experiments. Scale bars, 100 μm.

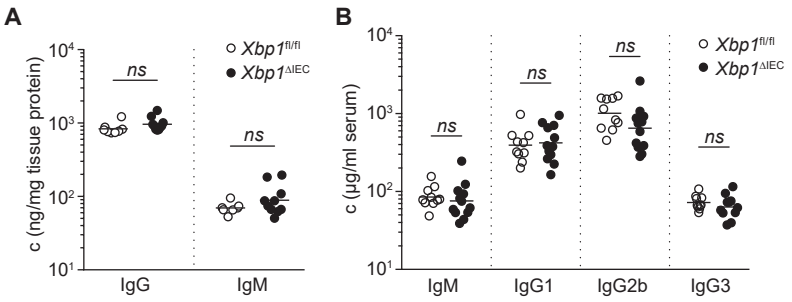

Fig. S2. The IEC ER stress induced immunoglobulin response is specific for IgA. (A) Ileal intra-tissue IgG and IgM concentrations (c, normalized by total soluble tissue protein) in *Xbp1*$^{\Delta IEC}$ mice *Xbp1*$^{fl/fl}$ controls ($n = 7–10$). **(B)** Serum immunoglobulin concentrations ($n = 10–12$). Symbols represent individual animals. Bars represent geometric means. *P*-values were calculated by unpaired Student's *t*-test. All data are representative of two independent experiments.

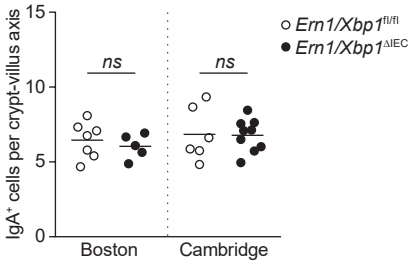

Fig. S3. IRE1α is critical for the IEC ER stress induced IgA response. Quantification of small-intestinal IgA$^+$ cells along ≥50 ileal crypt-villus axes (n = 5–9). Data represent two independent cohorts that were housed in the indicated facilities. Symbols represent individual animals. Bars represent arithmetic means. *P*-values were calculated by unpaired Student's *t*-test.

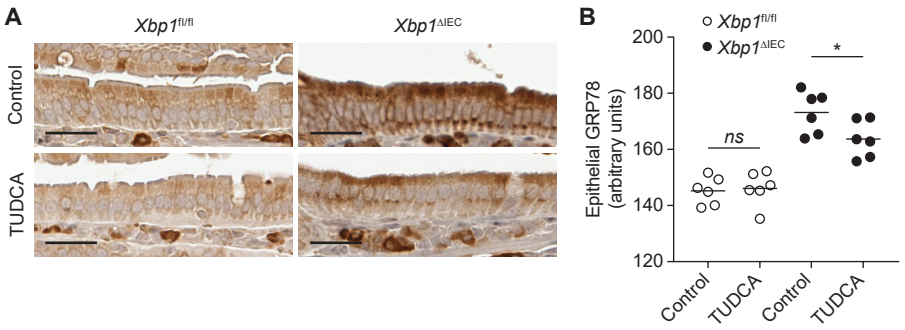

Fig. S4. Treatment of *Xbp1*$^{\Delta IEC}$ mice with TUDCA reduces epithelial ER stress. **(A)** Representative IHC images for GRP78 (brown) in ileal tissue of *Xbp1*$^{\Delta IEC}$ mice and *Xbp1*$^{fl/fl}$ controls after treatment with either TUDCA (2 mg/ml) in the drinking water or plain water (control) for two weeks. **(B)** Quantification of epithelial GRP78 staining intensity ($n=6$, data from one experiment). Scale bars, 20 μm. Symbols represent individual animals. Bars represent arithmetic means. *P*-values were calculated by two-way ANOVA with Fishers LSD method and two-stage step-up method of Benjamini, Krieger and Yekutieli to control the false discovery rate. *$P<0.05$, **$P<0.01$, ***$P<0.001$.

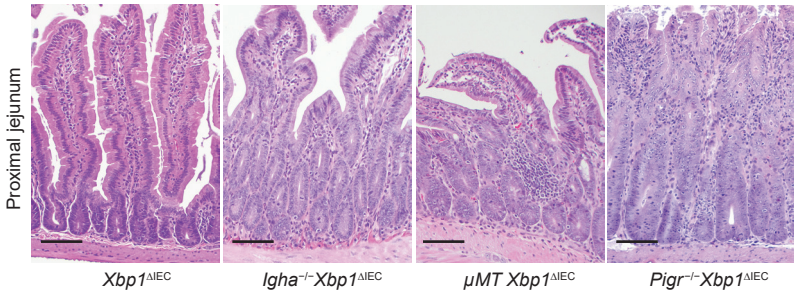

Fig. S5. Jejunal enteritis in *Xbp1*$^{\Delta IEC}$ mice that lack IgA, B cells or the pIgR. H&E staining of the proximal jejunum of the indicated genotypes. Images are representative of the corresponding groups depicted in Fig. 1J, K and O (n = 4–26, data pooled from 4 independent cohorts). Scale bars, 100 μm.

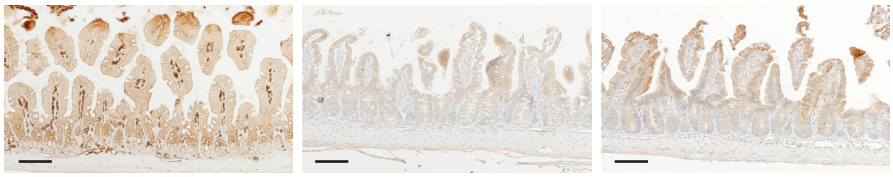

Fig. S6. No small-intestinal LP IgA$^+$ cells in *μMT Xbp1*$^{\Delta IEC}$ mice. Representative IHC images for IgA (brown) in ileal sections of C57BL/6J, *μMT Xbp1*$^{fl/fl}$ and *μMT Xbp1*$^{\Delta IEC}$ mice ($n=2$). Data are representative of two independent experiments. Scale bars, 100 μm.

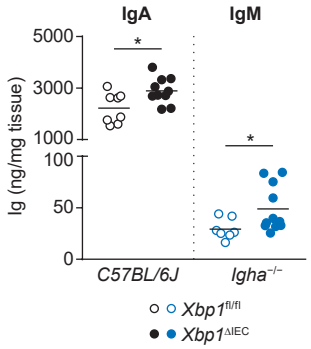

Fig. S7. *Igha*$^{-/-}$*Xbp1*$^{\Delta IEC}$ mice exhibit low levels of compensatory tissue IgM. Symbols represent individual animals (n=7–11). Data are representative of two independent experiments. IgA concentrations (per mg of SI tissue) from C57BL/6J *Xbp1*$^{\Delta IEC}$ mice as presented in Fig. 1B are shown for comparison. Bars represent arithmetic means. *P*-values were calculated by unpaired Student's *t*-test. *P<0.05, **P<0.01, ***P<0.001.

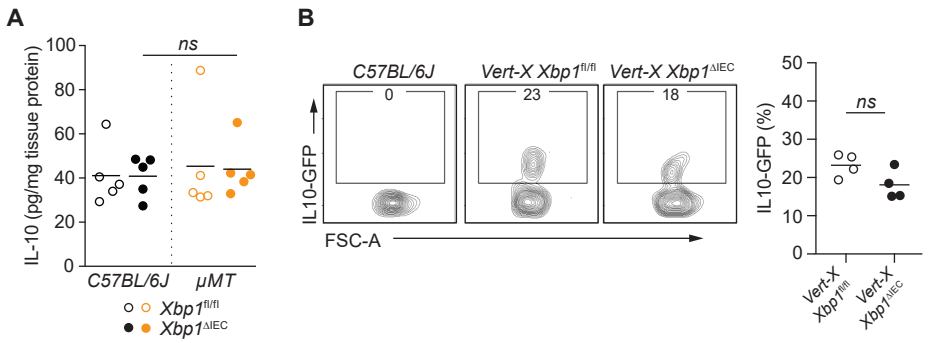

Fig. S8. The IEC ER stress induced IgA response is not associated with increased IL-10. **(A)** Ileal tissue IL-10 normalized by total soluble tissue protein ($n=5$, one experiment). **(B)** Representative plots and frequencies of IL-10 reporter$^+$ B cells (gated on CD45$^+$CD19$^+$ LP lymphocytes) in the indicated genotypes ($n=4$, one experiment). Symbols represent individual animals. Bars represent arithmetic means. *P*-values were calculated by one-way ANOVA (A) or unpaired Student's *t*-test (B).

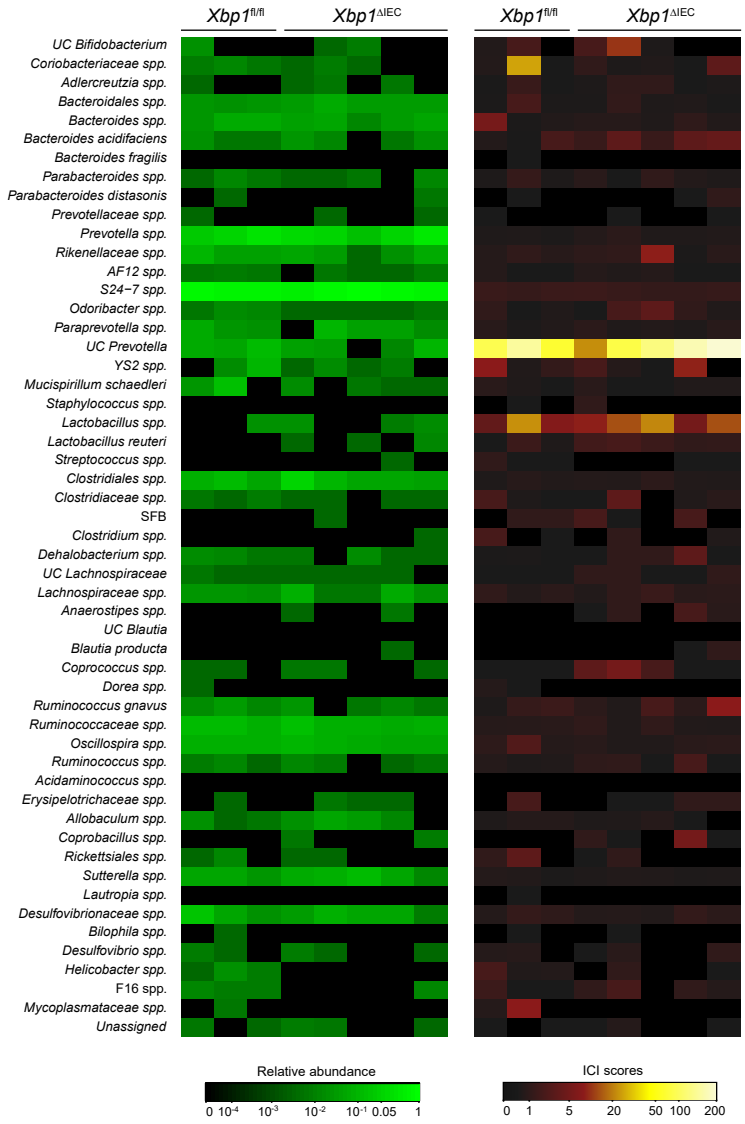

Fig. S9. No differences in IgA coating of fecal bacteria between *Xbp1*$^{\Delta IEC}$ mice and *Xbp1*$^{fl/fl}$ controls. Heatmaps of IgA-SEQ results depict relative abundance of genera in the fecal samples (pre-sort) and their IgA coating index (ICI). Each column represents an individual animal of the indicated genotype ($n = 3–5$, one experiment).

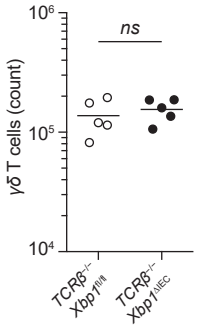

Fig. S10. No increase of compensatory γδ T cells in ***TCRβ*$^{-/-}$*Xbp1*$^{\Delta IEC}$ **mice.** Absolute counts of small-intestinal lamina propria γδ T cells (CD45^{+}TCRγδ^{+}) in *TCRβ*$^{-/-}$*Xbp1*$^{fl/fl}$ and *TCRβ*$^{-/-}$*Xbp1*$^{\Delta IEC}$ mice ($n=5$, one experiment). Symbols represent individual animals. Bars represent geometric means. *P*-values were calculated by unpaired Student's *t*-test.

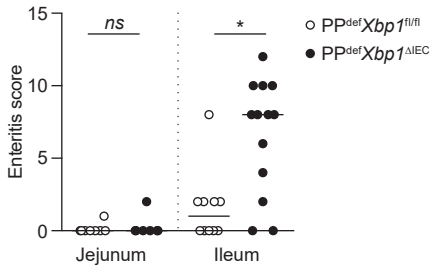

Fig. S11. PP-deficient *Xbp1*$^{\Delta IEC}$ mice do not develop spontaneous jejunal inflammation. Small-intestinal inflammation scores of Peyer's patch–deficient (PP^{def}) *Xbp1*$^{\Delta IEC}$ mice and *Xbp1*$^{fl/fl}$ controls ($n = 7–13$). Symbols represent individual animals. Bars represent medians. Data are compiled from two independent experiments. *P*-values were calculated by Mann–Whitney *U* test. **P* < 0.05, ***P* < 0.01, ****P* < 0.001.

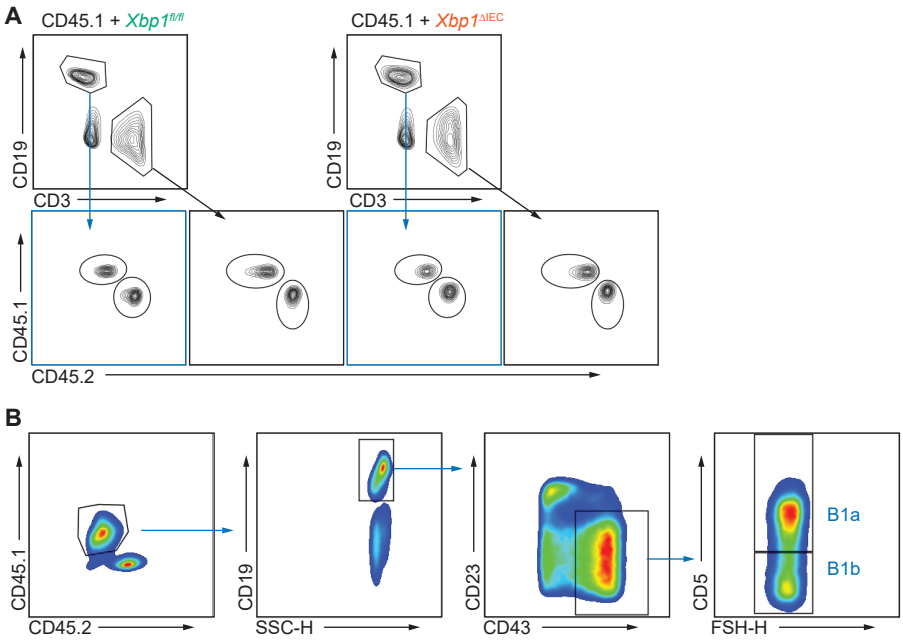

Fig. S12. Gating strategy for parabiosis experiment. (A) Gating of blood B and T cells. **(B)** Gating of peritoneal B1a and B1b cells**.** Plots are representative of all animals from the parabiotic experiment ($n = 7–8$ pairs per genotype).

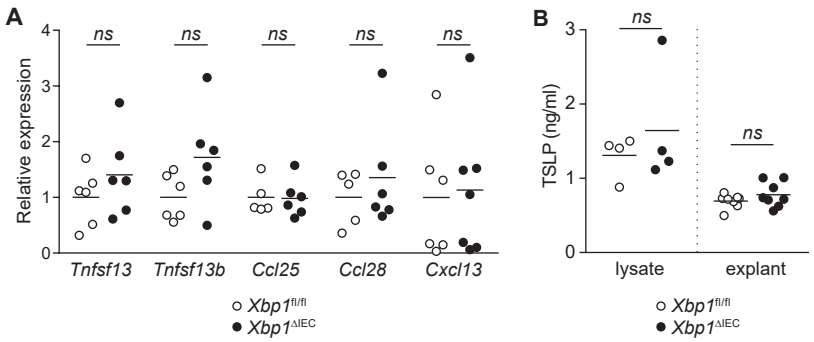

Fig. S13. Similar expression of cytokines associated with IgA class switching and plasma cell recruitment in in *Xbp1*$^{\Delta IEC}$ mice and *Xbp1*$^{fl/fl}$ controls. (A) Quantitative RT-PCR expression analysis of the noted cytokines (normalized to *Gapdh*) in SI tissue of *Xbp1*$^{\Delta IEC}$ mice and *Xbp1*$^{fl/fl}$ controls ($n = 5–7$, one experiment). **(B)** Concentration of TSLP in SI tissue lysates ($n = 4$, one experiment) or supernatant of SI explant cultures ($n = 8$, one experiment) of *Xbp1*$^{\Delta IEC}$ mice and *Xbp1*$^{fl/fl}$ controls. Symbols represent individual animals. Bars represent arithmetic means. *P*-values were calculated by unpaired Student's *t*-test.

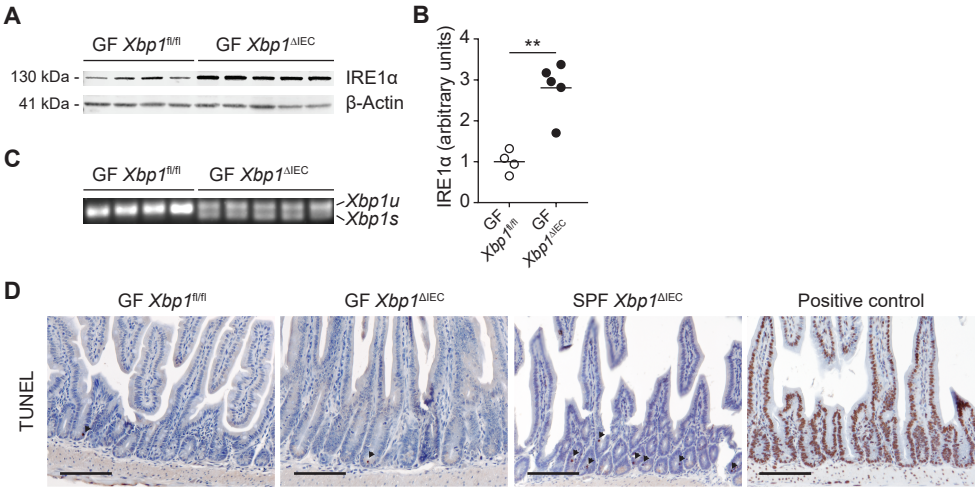

Fig. S14. Germ-free *Xbp1*$^{\Delta IEC}$ mice exhibit small-intestinal ER stress but low rates of apoptotic events. (A) Immunoblot of whole-thickness SI tissue lysates from GF *Xbp1*$^{\Delta IEC}$ mice and GF *Xbp1*$^{fl/fl}$ controls for IRE1α (n=4–5, data from one experiment). **(B)** Densitometry of (A), normalized to β-Actin. **(C)** *Xbp1* splicing in whole-thickness SI tissue samples from GF *Xbp1*$^{\Delta IEC}$ mice and GF *Xbp1*$^{fl/fl}$ controls (n=4–5, data from one experiment). *Xbp1u*, unspliced form (171 bp). *Xbp1s*, spliced form (145 bp). **(D)** Representative images of TUNEL-labeled SI sections of the indicated genotypes and housing conditions. Positive control was obtained by nuclease treatment of sections. The experiment was performed once. Symbols represent individual animals. Bars represent arithmetic means. *P*-values were calculated by unpaired Student's *t*-test. Scale bars, 100 μm.

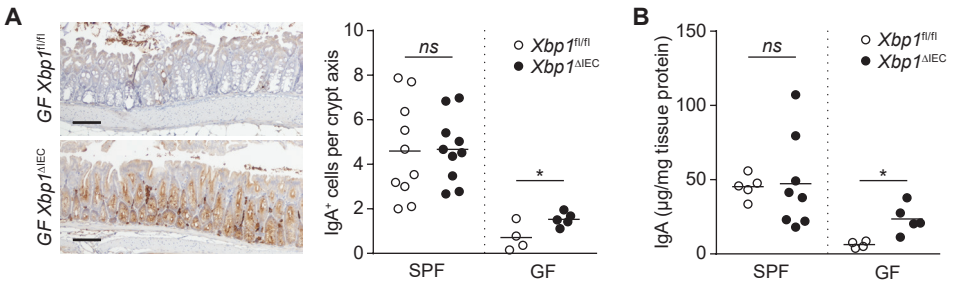

Fig. S15. Germ-free but not SPF *Xbp1*$^{\Delta IEC}$ mice show increased numbers of colonic IgA plasma cells and levels of tissue IgA. (A) Representative IHC images and quantification of colonic LP IgA^{+} cells (brown) along ≥50 crypts (n=4–10, one experiment). **(B)** Colonic intra-tissue IgA normalized by total soluble tissue protein (n=4–8, one experiment). Scale bars, 100 µm. Symbols represent individual animals. Bars represent arithmetic means. P-values were calculated by unpaired Student's t-test. *P<0.05, **P<0.01, ***P<0.001.


A
0 1 2 3 4 5 6 7 8 9 10 11 12 13 14
Cxcl13
Vsig4
Pf4
Timd4
Marco
Arg1
Saa3
C4b
Adgre1
Sdc3
Slpi
Apoe
Lyz2
Alox15
Cd9
Ccl24
C1qc
C1qa
C1qb
Fabp5
Plac8
Ly6a
Mzb1
S100a6
Ms4a1
Cd79a
Dnajc7
Siglecg
Cd79b
Ebf1
Ly6d
Fcmr
Ltb
Cd74
Ptprcap
Ccr7
H2−DMb2
Napsa
Zcwpw1
Prg4
Map1lc3a
Bri3
Trf
Timp2
Fabp4
Khk
Folr2
Ccl6
F13a1
Retnla
Ccl9
Fcna
Pltp
Wfdc17
Lyz1
Actb
Notch2
Slc39a1
Dusp3
Fam46a
Itga6
Nfia
Prtn3
Padi4
Ms4a4b
Cd3d
Ms4a6b
Cd3g
Bcl2
Gimap3
Tmsb10
Ccl5
Ccr2
Fcrls
H2−DMb1
Psap
H2−Eb1
H2−Aa
H2−Ab1
Stmn1
2810417H13Rik
Mcm6
Gmnn
Dut
Ranbp1
Siva1
H2afz
Tuba1b
Nkg7
Ly6c2
Cd8b1
AW112010
Cd209a
Plbd1
Mgl2
Gm2a
Tmem176a
Top2a
Birc5
Ube2c
Hist1h2ap
Mki67
Hmgb2
Tubb5
Lef1
Dapl1
Lck
Saraf
B
Cluster
0 1 2 3 4 5 6 7 8 9 10 11 12 13 14
Csf1r
Adgre1
Itgam
Icam2
Timd4
H2−Aa
Retnla
Ccr2
Cd209a
Mki67
Top2a
Map1lc3a
Folr2
Notch2
Ms4a1
Cd79a
Fcer2a
Fcmr
Lifr
Cd3e
Cd4
Nkg7

Fig. S16. Single-cell RNA sequencing reveals transcriptional identities of peritoneal cavity cells in germ-free mice. (A) Heatmap showing expression of top 10 marker genes (z-score −2.5 to +2.5; blue to red) by cluster as defined in Fig. 3F. **(B)** Violin plots showing expression probability distributions of selected genes across clusters as defined in Fig. 3F. Note the high expression of *Lifr* and low expression of *Fcmr* in cluster 2, consistent with a B1b transcriptional phenotype as previously described (immgen.org). Both panels depict the aggregated data obtained from germ-free $Xbp1^{\Delta IEC}$ and $Xbp1^{fl/fl}$ mice ($n = 11{,}104$ cells). The experiment was performed once.

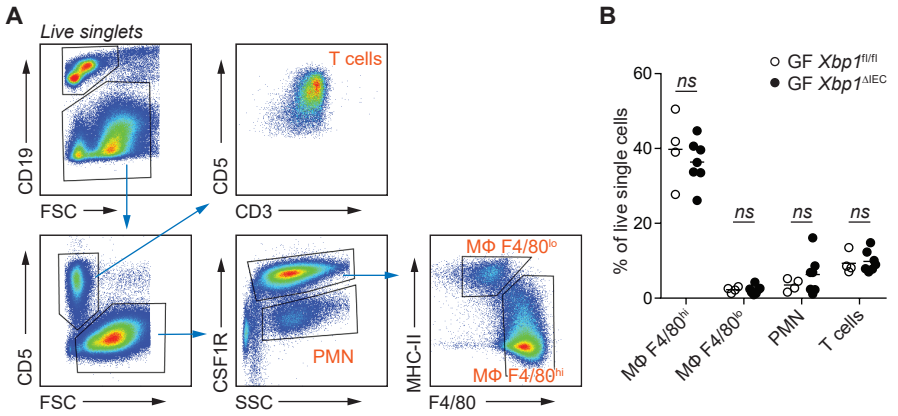

Fig. S17. No differences in peritoneal myeloid and T cells between GF *Xbp1*$^{\Delta IEC}$ mice and GF *Xbp1*$^{fl/fl}$ controls. (A) Gating strategy. **(B)** Frequencies of myeloid and T cells among peritoneal cavity cells of GF *Xbp1*$^{\Delta IEC}$ mice and GF *Xbp1*$^{fl/fl}$ controls ($n = 4–7$). Data are representative of two independent experiments. MΦ, macrophages. PMN, polymorphonuclear leukocytes. Symbols represent individual animals. Bars represent arithmetic means. *P*-values were calculated by unpaired Student's *t*-test.

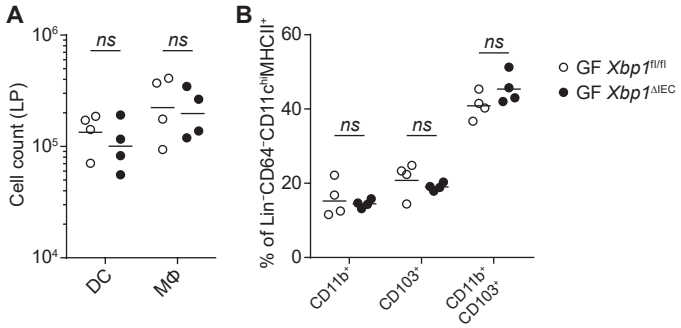

Fig. S18. No differences in small-intestinal LP myeloid cell populations between GF *Xbp1*$^{\Delta IEC}$ mice and GF *Xbp1*$^{fl/fl}$ controls. (A) Absolute counts of small-intestinal LP dendritic cells (DC, CD45$^+$CD3$^-$CD19$^-$NK1.1$^-$Ly6G$^-$CD64$^-$MHCII$^+$CD11c^{hi}) and macrophages (MΦ, CD45$^+$CD3$^-$CD19$^-$NK1.1$^-$Ly6G$^-$CD64$^+$) in GF *Xbp1*$^{\Delta IEC}$ mice and GF *Xbp1*$^{fl/fl}$ controls ($n = 4$, one experiment). **(B)** Frequencies of CD11b$^+$, CD103$^+$ and CD11b$^+$CD103$^+$ subsets of small-intestinal LP DCs. Gating strategy as described previously (*49*). Symbols represent individual animals. Bars represent geometric means (A) or arithmetic means (B). *P*-values were calculated by unpaired Student's *t*-test.

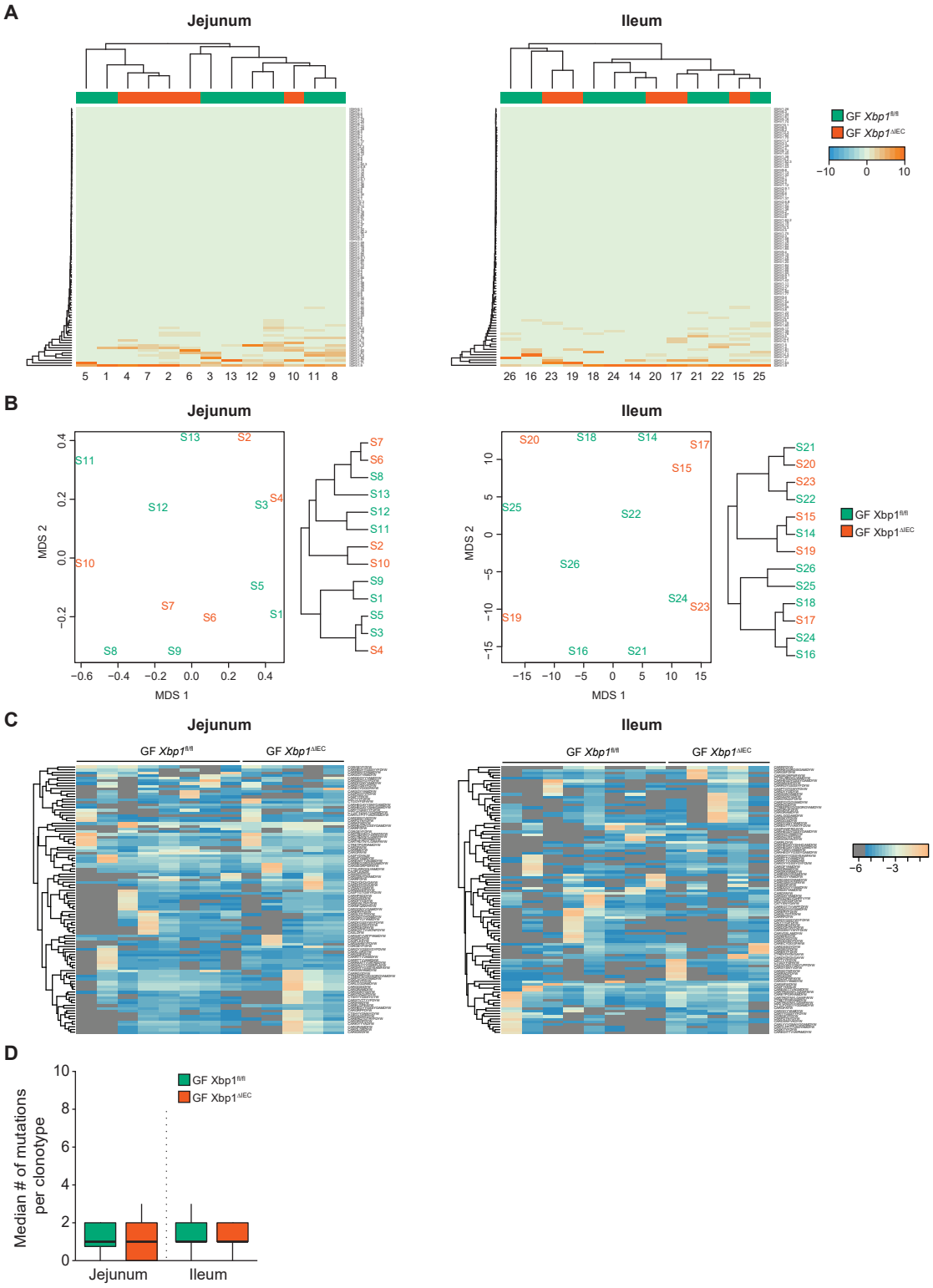

Fig. S19. IgA repertoire analysis of small-intestinal LP cells from germ-free *Xbp1*$^{\Delta IEC}$ mice confirms a polyclonal IgA response. (A) Heatmap depicting variable segment usage in IgA from jejunal (left) and ileal (right) samples of germ-free (GF) *Xbp1*$^{\Delta IEC}$ and *Xbp1*$^{fl/fl}$ mice ($n = 5–8$,

experiment performed once). Each column represents an individual animal of the indicated genotype. Color indicates column z-score. **(B)** Repertoire overlap as assessed by cluster analysis using multi-dimensional scaling (MDS) and hierarchical clustering. The geometric mean of relative overlap frequencies of clonotypes (defined by exact match of CDR3 amino acid sequences) was used as an overlap metric. **(C)** Heatmap depicting the abundance of the Top100 shared clonotypes between the different mice. Each column represents an individual animal of the indicated genotype. **(D)** Mutation load expressed as the median number of mutations per clonotype.

Supplementary Tables

Table S1: Antibodies used for flow cytometry.

Target	Clone	Fluorochromes	Vendor	Dilution
CD3	17A2	APC/Cy7, FITC, PerCP/Cy5.5	Biolegend	1:100
CD5	53-7.3	APC	BD	1:200
CD11b	M1/70	eFluor 450	eBioscience	1:400
CD11c	N418	PE/Cy7	Biolegend	1:400
CD19	6D5	APC/Cy7, PE	Biolegend	1:200
CD23	B3B4	PE/Cy7	Biolegend	1:200
CD43	eBioR2/60	PE	eBioscience	1:200
CD45	30-F11	Alexa Fluor 700	Biolegend	1:800
CD45.1	A20	BV605	Biolegend	1:800
CD45.2	104	BV786	BD	1:400
CD45R/B220	RA3-6B2	PE/Cy7	Biolegend	1:400
CD64	X54-5/7.1	APC	Biolegend	1:200
CD95	Jo2	PE	Biolegend	1:100
CD103	M290	PE	BD	1:200
CD115 (CSF1R)	AFS98	FITC	Thermo Fisher	1:100
CXCR5	2G8	Biotin	eBioscience	1:50
F4/80	BM8	APC/Cy7, FITC	Biolegend	1:200
GL7	GL7	FITC	Biolegend	1:100
I-A/I-E	M5/114.15.2	Alexa Fluor 700	eBioscience	1:200
IgA	C10-3	Alexa Fluor 647†, FITC	BD	1:800–1:1,200*
IgM	R6-60.2	FITC	BD	1:800
Ly6G	1A8	APC/Cy7	Biolegend	1:400
NK-1.1	PK136	APC/Cy7	Biolegend	1:100
PD-1	29F.1A12	FITC	Biolegend	1:100
TCRβ	H57-597	eFluor 450, FITC	eBioscience	1:100
TCRγ/δ	GL3	APC	Biolegend	1:100

*intracellular staining, †custom conjugation (Alexa Fluor 647 Labeling Kit, Molecular probes).

Table S2: Antibodies used for immunoglobulin ELISA.

Target	Capture antibody	Detection antibody (HRP)
IgM	1020-01, SouthernBiotech, 1 µg/µl	A8786, Sigma-Aldrich, 1:1,000
	or A90-101A, Bethyl, 10 µg/µl	A90-101P, Bethyl, 1:50,000
IgG1	1070-01, SouthernBiotech, 1 µg/µl	A3673, Sigma-Aldrich, 1:1,000
IgG2a	1080-01, SouthernBiotech, 1 µg/µl	A3673, Sigma-Aldrich, 1:1,000
IgG2b	1090-01, SouthernBiotech, 1 µg/µl	A3673, Sigma-Aldrich, 1:1,000
IgG3	1100-01, SouthernBiotech, 1 µg/µl	A3673, Sigma-Aldrich, 1:1,000
IgG-Fc	A90-131A, Bethyl, 10 µg/µl	A90-131P, Bethyl, 1:50,000
IgA	1040-01, SouthernBiotech, 1 µg/µl	A4789, Sigma-Aldrich, 1:1,000
	or A90-103A, Bethyl, 10 µg/µl	A90-103P, Bethyl, 1:20,000

Fig. 1

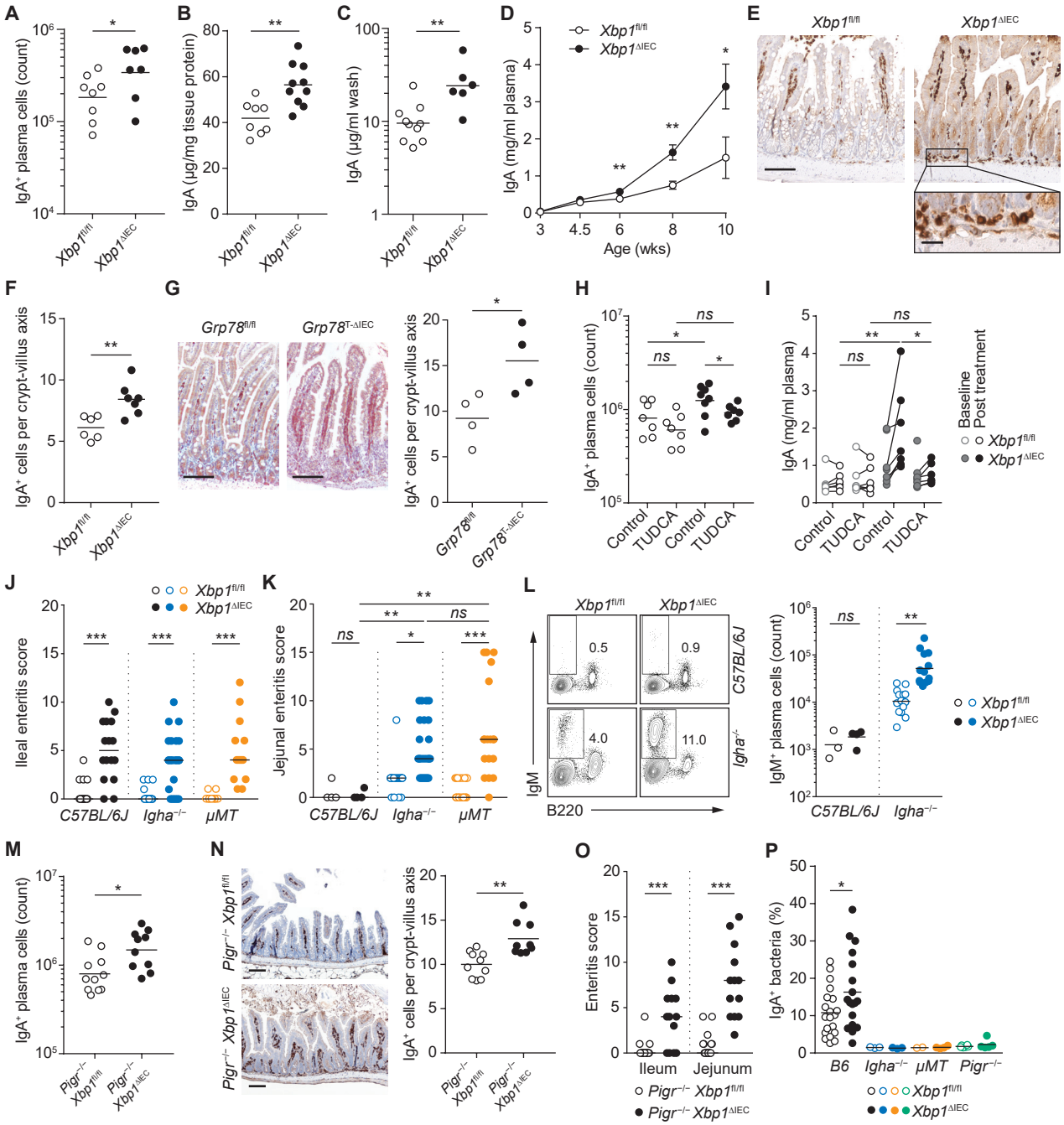
A
IgA+ plasma cells (count)
Xbp1fl/fl
Xbp1ΔIEC
B
IgA (μg/mg tissue protein)
C
IgA (μg/ml wash)
D
IgA (mg/ml plasma)
Age (wks)
E
F
IgA+ cells per crypt-villus axis
G
Grp78fl/fl
Grp78T-ΔIEC
H
Control
TUDCA
I
Baseline
Post treatment
J
Ileal enteritis score
C57BL/6J
Igha−/−
μMT
K
Jejunal enteritis score
L
IgM
B220
C57BL/6J
Igha−/−
IgM+ plasma cells (count)
M
Pigr−/−
N
O
Enteritis score
Ileum
Jejunum
P
IgA+ bacteria (%)
B6

Fig. 2

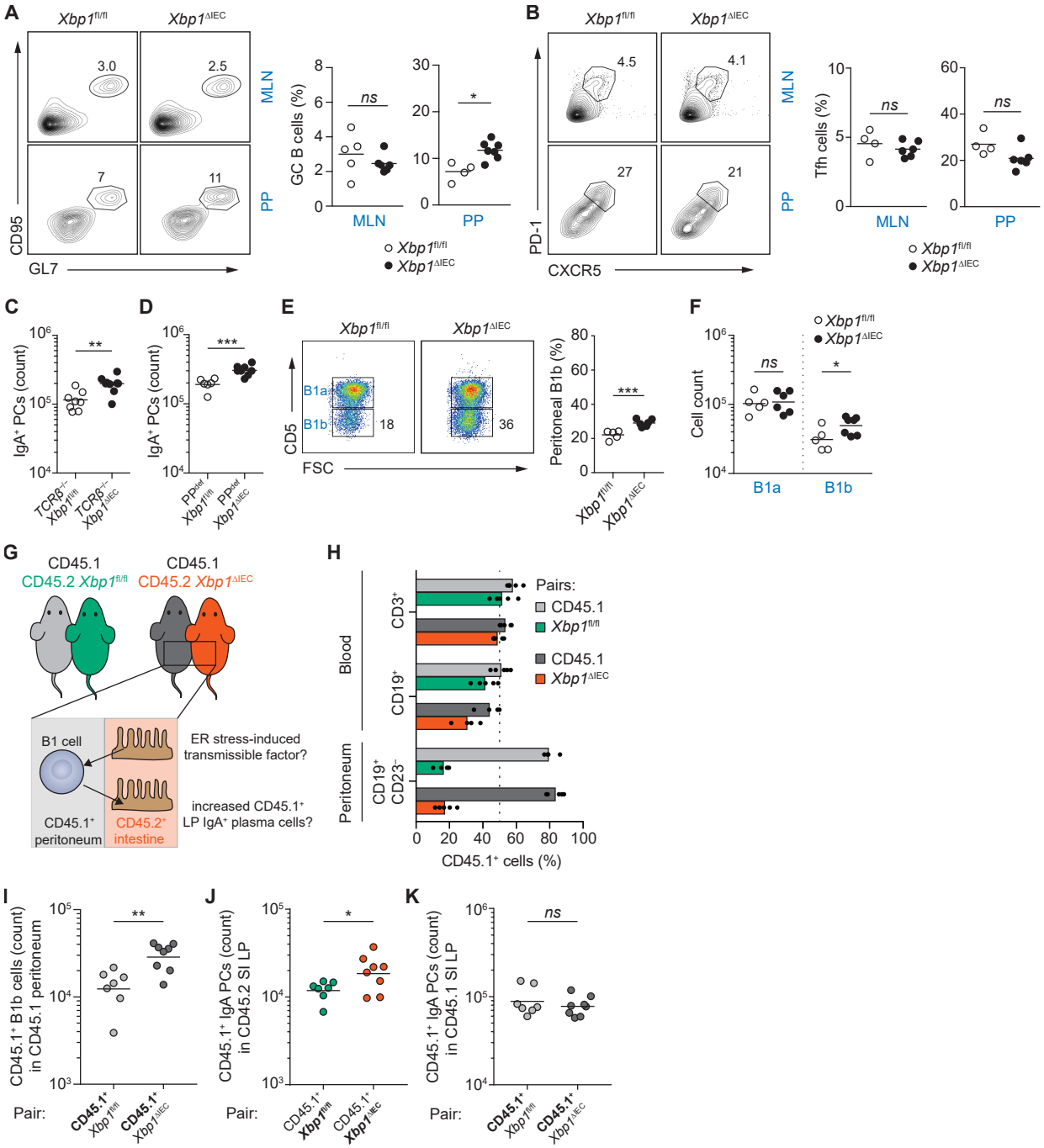
A
B
C
D
E
F
G
H
I
J
K
Xbp1fl/fl
Xbp1ΔIEC
MLN
PP
CD95
GL7
PD-1
CXCR5
GC B cells (%)
Tfh cells (%)
IgA+ PCs (count)
Peritoneal B1b (%)
Cell count
B1a
B1b
CD5
FSC
ns
CD45.1
CD45.2 Xbp1fl/fl
CD45.2 Xbp1ΔIEC
B1 cell
CD45.1+ peritoneum
CD45.2+ intestine
ER stress-induced transmissible factor?
increased CD45.1+ LP IgA+ plasma cells?
Blood
Peritoneum
CD3+
CD19+
CD19+ CD23−
Pairs:
CD45.1+ cells (%)
CD45.1+ B1b cells (count) in CD45.1 peritoneum
CD45.1+ IgA PCs (count) in CD45.2 SI LP
CD45.1+ IgA PCs (count) in CD45.1 SI LP
Pair:

Fig. 3

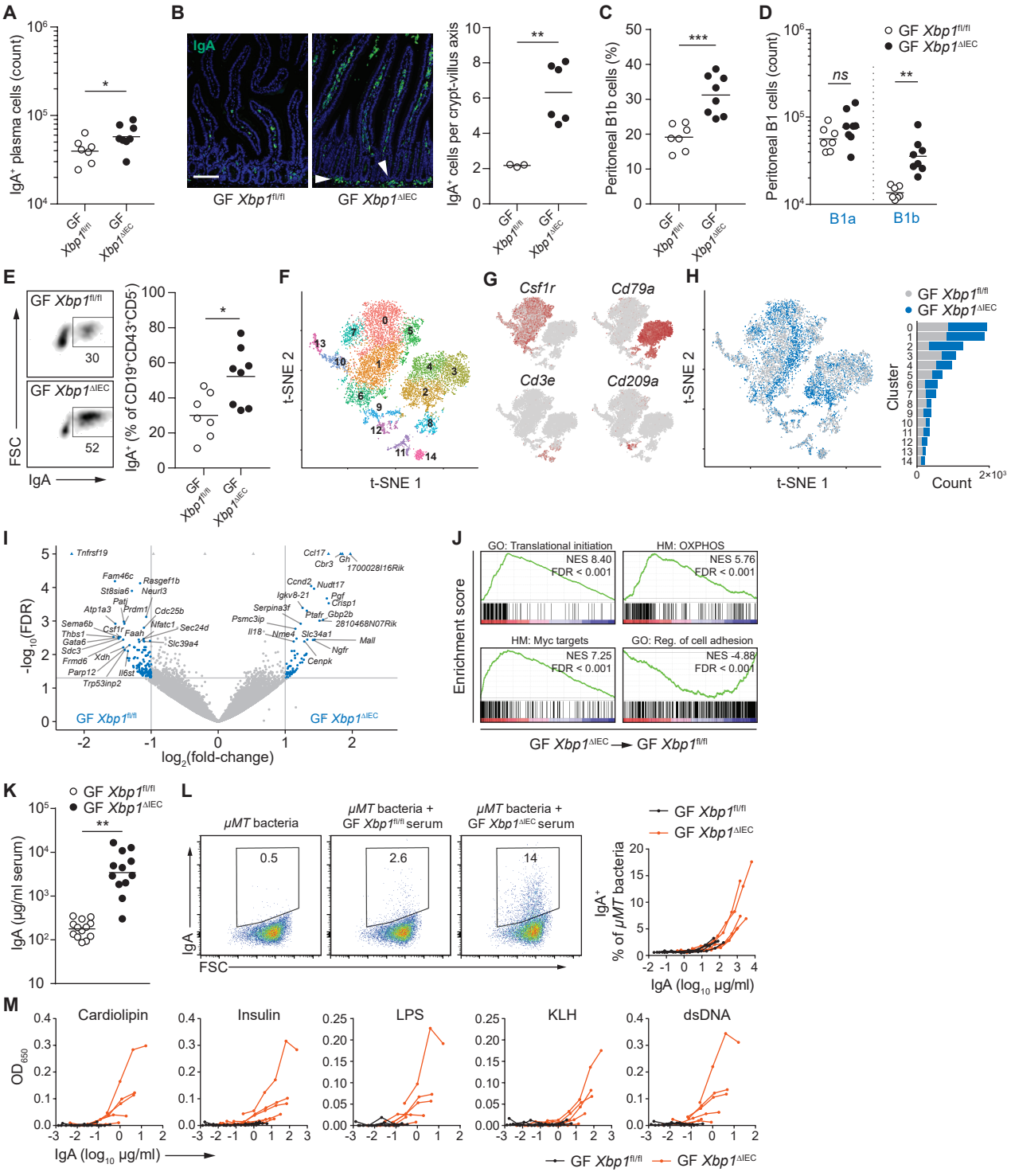
A
IgA+ plasma cells (count)
GF Xbp1fl/fl
GF Xbp1ΔIEC
B
IgA
GF Xbp1fl/fl
GF Xbp1ΔIEC
IgA+ cells per crypt-villus axis
C
Peritoneal B1b cells (%)
D
Peritoneal B1 cells (count)
ns
B1a
B1b
E
FSC
IgA
30
52
IgA+ (% of CD19+CD43+CD5-)
F
t-SNE 1
t-SNE 2
G
Csf1r
Cd79a
Cd3e
Cd209a
H
Cluster
Count
I
-log10(FDR)
log2(fold-change)
Tnfrsf19
Ccl17
Ccr3
Gh
1700028I16Rik
Fam46c
Rasgef1b
St8sia6
Neurl3
Patl
Atp1a3
Prdm1
Cdc25b
Sema6b
Csf1r
Faah
Nfatc1
Sec24d
Thbs1
Gata6
Slc39a4
Sdc3
Frmd6
Xdh
Parp12
Il6st
Trp53inp2
Ccnd2
Nudt17
Igkv8-21
Pgf
Crisp1
Serpina3f
Ptafr
Gbp2b
Psmc3ip
2810468N07Rik
Il18
Nme4
Slc34a1
Mall
Ngfr
Cenpk
J
GO: Translational initiation
NES 8.40
FDR < 0.001
HM: OXPHOS
NES 5.76
FDR < 0.001
HM: Myc targets
NES 7.25
FDR < 0.001
GO: Reg. of cell adhesion
NES -4.88
FDR < 0.001
Enrichment score
GF Xbp1ΔIEC → GF Xbp1fl/fl
K
IgA (μg/ml serum)
L
μMT bacteria
μMT bacteria + GF Xbp1fl/fl serum
μMT bacteria + GF Xbp1ΔIEC serum
0.5
2.6
14
IgA
FSC
IgA+ % of μMT bacteria
IgA (log10 μg/ml)
M
Cardiolipin
Insulin
LPS
KLH
dsDNA
OD650
IgA (log10 μg/ml)

Fig. 4

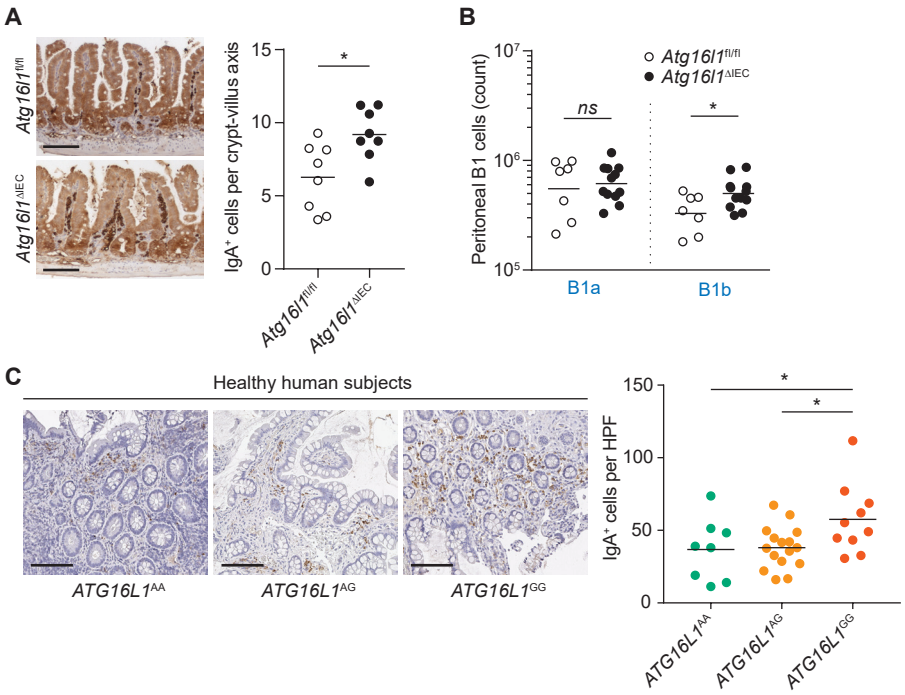
A
Atg16l1fl/fl
Atg16l1ΔIEC
IgA+ cells per crypt-villus axis
15
10
5
0
*
Atg16l1fl/fl
Atg16l1ΔIEC
B
Peritoneal B1 cells (count)
10^7
10^6
10^5
Atg16l1fl/fl
Atg16l1ΔIEC
ns
*
B1a
B1b
C
Healthy human subjects
ATG16L1AA
ATG16L1AG
ATG16L1GG
IgA+ cells per HPF
150
100
50
0
*
*
ATG16L1AA
ATG16L1AG
ATG16L1GG